Fall 2018

Nonlinear Stiffness and Viscoelasticity of Inhibitor-Treated Blood Clots by Tensile Testing

Wilson S. Eng
San Jose State University

NONLINEAR STIFFNESS AND VISCOELASTICITY OF INHIBITOR-TREATED BLOOD CLOTS BY TENSILE TESTING

A Thesis

Presented to

The Faculty of the Department of Mechanical Engineering

San José State University

In Partial Fulfillment

of the Requirements for the Degree

Master of Science

by

Wilson S. Eng

December 2018

The Designated Thesis Committee Approves the Thesis Titled

NONLINEAR STIFFNESS AND VISCOELASTICITY OF INHIBITOR-TREATED BLOOD CLOTS BY TENSILE TESTING

by

Wilson S. Eng

APPROVED FOR THE DEPARTMENT OF MECHANICAL ENGINEERING

SAN JOSÉ STATE UNIVERSITY

December 2018

Sang-Joon Lee, Ph.D.	Department of Mechanical Engineering
Anand Ramasubramanian, Ph.D.	Department of Chemical and Materials Engineering
Amit Saha, Ph.D.	Stanford University School of Medicine

ABSTRACT

NONLINEAR STIFFNESS AND VISCOELASTICITY OF INHIBITOR-TREATED BLOOD CLOTS BY TENSILE TESTING

by Wilson S. Eng

Although blood clots are vital to wound healing, little is known about what factors influence clot stiffness and dynamic response. This work investigates the mechanics of inhibitor-treated clots by direct tensile testing using a custom designed system for forces below 1 N. Inhibitors that affect clot formation include blebbistatin, which affects myosin II movement on actin, and cytochalasin D, which affects actin polymerization. The hypothesis of this investigation is that blebbistatin will have a greater effect on mechanical behavior than cytochalasin D, because the inhibition of myosin II will weaken the overall clot more than actin. This hypothesis was investigated using clots that were treated with blebbistatin and cytochalasin, using untreated whole blood as a reference. Clots were tested from five different donors with at least two replicates from each donor. Each clot was subjected to an initial stretch ratio of 1.5 to measure nonlinear stiffness, followed by a series of 1 mm increments to record stress relaxation. At a stretch ratio of 1.5, blebbistatin-treated clots exhibited 4.3% lower tensile stress than cytochalasin-treated clots. The relaxation time constant for blebbistatin-treated clots was 10% faster than for cytochalasin-treated clots. This evidence supports the hypothesis about the role of myosin II in blood and introduces experimental methodology that can be extended to studies on mechanics of other soft biological tissues.

ACKNOWLEDGMENTS

This work was supported in part by the Kordestani Endowment to the Charles W. Davidson College of Engineering at San José State University (SJSU) and in part by the AHA Institutional Research Enhancement Award (AIREA) program of the American Heart Association (Award Number 18AIREA33960524). I would like to thank Dr. Anand Ramasubramanian for providing background on the project and direction needed in testing blood clots. I would like to thank Dr. Amit Saha for his support with the specimen testing development. I would like to thank Dr. Sang-Joon (John) Lee for tirelessly providing guidance throughout the entire project and reviewing. I would like to thank members of the MEMS Lab at SJSU for help with fabrication and testing. Finally, I would like to thank my friends and family for their support.

TABLE OF CONTENTS

LIST OF TABLES

LIST OF FIGURES

LIST OF SYMBOLS

Symbol	Description
A	Cross-sectional area (mm²)
C_1	First Mooney-Rivlin parameter (Pa)
C_2	Second Mooney-Rivlin parameter (Pa)
F	Force (N)
h	Distance of specimen to load cell
k_L	Stiffness of load cell (N/m)
k_s	Stiffness of specimen (N/m)
k_{eq}	Stiffness of total system (N/m)
k_1	Stiffness of spring in lumped parameter (N/m)
k_2	Stiffness of spring in lumped parameter (N/m)
L	Total length travel (mm)
L_o	Original length of the specimen (mm)
t	Thickness of the specimen (mm)
u	Uncertainty
u_A	Area uncertainty (mm²)
u_F	Force uncertainty
u_{kL}	Load cell stiffness uncertainty (N/m)
u_t	Thickness uncertainty (μm)
u_w	Width uncertainty (μm)
$u_{\delta L}$	Load cell displacement uncertainty (μm)
u_σ	Stress uncertainty (Pa)
w	Width of the specimen (mm)
δ_s	Elongation of specimen (mm)
δ_L	Tip deflection of cantilever load cell (mm)
δ_{total}	Displacement of actuator (mm)
ε	Sine error
η	Damping values in lumped parameter (N·s/m)
θ	Angle of the sine error
σ	Stress (Pa)
τ	Time constant (s)

1. INTRODUCTION

1.1 Background

Blood clots are critical to preventing incessant bleeding, thus saving lives. The mechanical properties of the clot are vital to damming blood flow. The macroscopic mechanical properties of a blood clot such as stress-strain response and yield strength are functions of the blood composition and extent of cross-linking. Cross-linking is affected by numerous factors, including levels of a coagulation enzyme known as factor XIII (FXIII). However, several studies over the past few years have shown that blood clots are mechanically and morphologically heterogeneous in microscale, and micromechanical behavior can have important consequences in pathophysiological events such as stroke [1].

Clots are biocomposite materials that are formed as liquid blood transforms into a viscoelastic state. Fibrin, a key structural component of blood, is a polymer chain that has been shown to shift from a random orientation to an aligned configuration when strained [2]. The unique restructuring trait allows the clot to be flexible, but also resilient to external forces [3]. However, mechanical testing of a clot is not a simple task. The fluid-like consistency of blood makes mechanical property testing with conventional macroscale instruments such as an Instron® universal testing system (Illinois Tool Works, Norwood Massachusetts, USA) difficult in terms of fixturing and small-force resolution. Krasokha et al. found that casting blood into a mold was helpful in compressive testing because of the known dimensions and cross-section [4]. However, even with a well-prescribed shape, the blood consistency is difficult for an experimental device to grasp,

requiring unconventional mounting techniques to contain the specimen within the apparatus. In order to perform more informative mechanical testing of blood clots, there is a need for a versatile and sensitive apparatus that can apply finely controlled tensometric (i.e., force measurement under prescribed displacement) or extensometric (i.e., displacement measurement under applied force) testing in a consistent way.

1.1.1 Blood Clotting Mechanics

Blood clots are complex and have many clotting factors and pathways that can create a clot. Virchow's triad, named after Rudolf Virchow, describes the three contributing causes to thrombosis which are stasis, vessel wall injury, and hypercoagulability [5]. Fluid flow plays a role in the formation of clots. For example, a higher concentration of platelets tends to occur in arterial clots, for which fluid flow tends to have a higher flow rate than in veins [6]. The first stage of clotting occurs when there is an open wound. Vasoconstriction of endothelial cells occurs, because of a lack of nitric oxide for vasodilation during injury. In the second stage, platelets gather to form a plug at the wound, but will not be cross-linked until after coagulation occurs to prevent further bleeding with a stronger clot [7]. In the coagulation cascade there are two pathways, known as the intrinsic pathway and extrinsic pathway. The intrinsic pathway is a slower process using collagen and requires contributing roles of factors FXII, FXI, FIX, and FX. The extrinsic pathway is a faster process requiring only FVII, tissue factor (TF), and FX. The intrinsic pathway and extrinsic pathway meet at FX to start the common pathway.

The blood stream contains enzymes that change prothrombin (FII) into thrombin via factor Xa (where the letter "a" indicates activator). Activated platelets are able to

rearrange their structure to attach to fibrinogen (FI) on neighboring platelets to create a stronger plug at the injured site [8]. Eventually a network of platelets is created and its strength is enhanced when thrombin converts the fibrinogen into a fibrin a mesh that helps prevent blood flow. The fibrin network is then strengthened with the introduction of FXIII, which cross-links the structure allowing for greater strain stiffening and viscoelastic stiffness of blood clots [9].

This study will focus on the common pathway, for which collagen and tissue factor are not involved with initiating the clotting process. Thrombin is the enzyme used to initiate the clotting process, after which the clot will form and contract over time. Two platelet components that provide hemostatic clot structure by working together are actin filaments and myosin II motor proteins [10]. The platelet's local actin-myosin cytoskeleton relationship will be investigated further with the use of blebbistatin as a known drug that inhibits myosin II [11] and cytochalasin D as a known drug that inhibits actin polymerization [12]. Blebbistatin was found to change the biconcavity shape of red blood cells (RBC) due to the inhibition of myosin II, indicating structural weakening [13], whereas cytochalasin D was found to also weaken the clots by capping actin filaments as shown through thromboelastography (TEG) which is a test for blood coagulation efficiency [14].

1.1.2 Mechanical Properties of Blood

Many engineering materials such as metals exhibit linearly elastic mechanical behavior that follow Hooke's law, for which displacement is proportional to force. However, blood clots behave differently, since the cross-linked fibrin network is strain

stiffening. The structural rearrangement of fibers results in tension that is not linearly proportional to the applied displacement. Hyperelastic models, such as Neo-Hookean model or Mooney-Rivlin model, are methods to describe the strain stiffening characteristic.

There is also a difference when a clot is held at a prescribed displacement, because stress relaxation will occur. Linearly elastic materials will exhibit a constant force when extended and held at a fixed strain below the yield strain of the material. In the stress relaxation of blood clots, however, tension decreases with time when the clot is held at a fixed displacement. Viscoelastic models are used to describe this stress relaxation phenomenon with the use of springs and dampers in various configurations. The most basic models are the Maxwell model, consisting of a spring and damper in series, and the Kelvin-Voigt model, consisting of a spring and damper in parallel. The Maxwell model is better for stress relaxation for which displacement is fixed and the mechanical elements encounter reduced force, and the Kelvin-Voigt model is better for creep for which force is fixed and the mechanical elements undergo changes in geometry. The work in this thesis will use the standard linear solid model, which is also known as a Zener or a Maxwell representation that combines the Maxwell model and Kelvin-Voigt model [15].

1.2 Hypothesis

The work in this thesis investigates nonlinear stiffness and viscoelastic response of blood clots by performing mechanical tensile testing of clots subjected to inhibitors. The hypothesis is that blebbistatin affects stiffness and viscoelastic response of a clot more

than cytochalasin D, because myosin II plays a larger role than actin in clot stiffness. Inhibition of myosin II with blebbistatin is expected to create a weaker clot.

Myosin II protein is composed of two intertwined myosin chains which act along actin filaments through an adenosine triphosphate (ATP) energy cycle. ATP binds to a myosin II that begins to release the attached actin. The ATP is converted to adenosine diphosphate (ADP), a phosphate and energy which winds the myosin like a spring to provide mechanical energy. When the phosphate is released from myosin, the stored energy from the myosin is released to move along the actin filament, thus contracting. Blebbistatin can cause the myosin II to have low affinity to attach to actin, disrupting the phosphate activation site, by binding to ATPase intermediate with ADP [16]. If the actin filament is capped with cytochalasin D, then the contractions from the myosin will be shorter. However, if there is no myosin II activity, then the membrane proteins will be unable to contract and can be easily deformed [17].

1.3 Significance

There is still much unknown about the mechanical properties of blood clots. Understanding the mechanical properties of blood clots is important because of the potentially informative benefit to medical interventions such as drug therapy or thrombectomy. Most prior work in mechanical characterization of blood clots has been done using either rheometry, which measures tangential stress on a surface, or at the nanoscale with atomic force microscopy (AFM), which focuses on individual clot components. Direct tensile testing as applied in this thesis will provide an under-investigated methodology for characterizing blood clot mechanics.

2. RELATED WORK

2.1 Mechanical Properties of Fibrin and Other Biomaterials

When fibrinogen and thrombin are combined, a fibrin polymer is formed. Fibrin is an important structural component of blood clots that plays a role in treating ischemic strokes and myocardial infarctions, but a balance is needed because too much fibrin can lead to thrombosis and too little allows for uncontrollable bleeding [18]. Fibrin plays a versatile role in wound healing and angiogenesis [19]. A specific use of fibrin is fibrin sealant which is used in surgery as a hemostatic agent, preventing blood loss [20]. Fibrin has viscoelastic properties which are important in understanding and treating thrombosis. Fine clots are simpler to measure, because the planarity creates a two dimensional interaction rather than a three dimensional interaction that is more complicated [21]. A strong clot will deform differently than a weak one due to the nonuniform strain stiffening network. Biological tissues and clots benefit from strain stiffening, which allows for larger deformations prior to rupture [22]. A fibrin network can be cross-linked with FXIII to create a stronger clot. Due to its versatility of strength and biocompatibility, fibrin is already used in biomedical implants and tissue engineering [18].

Hydrogels are biomaterials consisting of water insoluble polymer chains with cross-linking properties [23]. Alginate is an example of a hydrogel material that exhibits mechanical behavior similar to the mechanical behavior of fibrin. Sodium alginate, a seaweed and kelp extract, has biocompatible characteristics that are favorable for wound healing and drug delivery systems. Alginate increases angiogenesis which helps facilitate the development of new blood cells increasingly for seven days [24]. Similar to fibrin,

alginate can be cross-linked ionically, thermally, covalently, and through cellular adhesion [25]. Drury et al. found that alginate ionically cross-linked with sodium chloride had stress-strain curves with an initial concavity upward for the strain stiffening portions of the plot [26]. When ionically cross-linked, alginate exhibits nonlinear stiffness similar to blood clots. A few other hydrogels such as heparin, chitosan, and agarose are also used in tissue engineering for their biocompatibility, biodegradability, and strain stiffening mechanical characteristics [23].

2.2 Methods for Mechanical Testing of Soft Materials

Soft biomaterials are typically small and difficult to handle. The consistency is similar to a gel, which can lead to slippage when trying to grasp mechanically. However, certain measurement techniques alleviate this issue of slippage. The test methodologies vary between apparatus types to bypass the specimen consistency. Rheometry uses the specimen soft gel consistency to measure material properties. Chemical adhesion holds the specimen in place and allows atomic force microscopy (AFM) to be used. A cast specimen allows for compression or tension testing. Electrowetting uses an electric field to manipulate the specimen into the desired configuration. The reviewed testing methods provide guidance on developed techniques to overcome slippage from grasping soft biomaterials.

2.2.1 Rheometry

A rheometer is a mechanical testing device that uses a rotating cone to compress the specimen in a medium at a prescribed rotational speed, thus providing mechanical characterization based on shear rate. Kim et al. studied fibrin, collagen, and fibrin-

collagen with a rheometer that compressed the specimens to 1/10 of the initial thickness to gather shear modulus information [27]. The shear elastic modulus G' and shear loss modulus G" are the typical properties that are reported from rheometry measurements. Wen et al. [22] found that an out of phase viscous response of G''is less than G' in cross-linked hydrogels, because nonlinear elasticity has a nonlinear stress and strain relationship. Polyacrylamide (PA) gels, for example, have G' increase with larger strains, indicating that strain stiffening is occurring. G' and G" are proportional to the stored elastic energy and the energy dissipated [28].

Ayala et al. studied the effects of cytochalasin D and blebbistatin on blood with rheometry [29]. A dosage dependency between 2.5 μM to 5.0 μM cytochalasin D and 5.0 μM to 10 μM blebbistatin was found, because the shear modulus continued to change [29]. If the shear modulus was steady, then the entire clot structure was inhibited. Tutwiler et al. tested whole blood by keeping the clot size at a constant volume with the rheometer and found that the increase in red blood cells weakens the clot contractile stress [30]. Rheometry methods proved to be useful in studying blood clots and inhibitor effects, but would not be able to measure actual tensile forces acting on soft biological materials.

2.2.2 Atomic Force Microscopy

In nanoscale, Markert et al. used AFM to test several biomaterials including alginate, collagen, and fibrin [31]. With AFM devices, a measured force can manipulate the specimen and image simultaneously. Studies by Feller showed that an AFM probe tip can adhere to blood and provide nanonewton force measurements with micron-scale

displacements by partially submerging the cantilever beam [32]. The nanometer scale allows for studying the mechanical properties of single components of a clot. Other methodologies can prepare the specimen for AFM such as electrospinning, which allows for a thinner fiber to be created [33]. However, larger networks in the macro scale are difficult to understand, because of the very fine resolution of AFM devices.

Examining a whole clot at macroscale, Lam et al. investigated the mechanics and dynamics of platelets with force measurements [34]. Crow et al. further introduced cytochalasin D and blebbistatin to understand the inhibitors effects on clot retraction [35]. When treated with a cytochalasin D concentration of 500 nM, clots contracted at 0.40 μm/min. When treated with a blebbistatin concentration of 30 μM, clots contracted at 0.24 μm/min. Clot contraction ceased while using 1 μM cytochalasin and 50 μM blebbistatin concentrations [35].

2.2.3 Compression Testing

Compression testing is another test methodology performed on biomaterials. Typically the test specimen will be in a holder and compressed to obtain relevant mechanical properties. This system benefits from the not having to grasp onto the soft biomaterial. Krasoskha et al. tested porcine blood by compression at 0.25 mm/s by a plate in a chamber where the clot takes the chamber shape [4]. Beyond 70% compression a strain stiffening effect was observed with a large increase in stress [4]. However, the methodology did not have a specified predetermined clot shape and chamber walls could have affected the results. There was no indication of a retraction period for the clot, such that the observations could have been more related to plasma rather than the actual clot.

In contrast with Murphy et al. who performed compression testing on round fibrin gel specimens between two plates on an Instron® universal testing machine [36]. The compression of the fibrin gel did not have any interference, because the gel was able to retain its own structure. The compression testing proved to be a simple way of testing clots, but tensile testing is more indicative of clots breaking apart in embolisms.

2.2.4 Tensile Testing

Flexures have been used to measure contraction and small movements in tensile testing. Known flexural stiffness allows for simple forces measurements with a known displacement. Polydimethylsiloxane (PDMS) strain sensing beams were used to measure clotting contraction forces with the Young's modulus of the flexure and displacement [37]. The same principles were used for flexures to study the strength of an onion skin in dry and wet conditions [38]. A similar experiment by Kim et al. [39] was done using a piezoelectric actuator and a flexure as the known force, a variation of the approach by Zamil et al. [38]. The flexure stiffness was known, allowing the onion movement to be measured.

Currently, there is no current standard for tensile testing soft biological materials such as hydrogels and fibrin. There are commercial products that can test soft biological tissue, such as the DMT wire myograph (Danish Myo Technology, Aarhus, Denmark). However, the device is specialized for loop arteries that attach to the two wires and are pulled apart. ADMET has a BioTense Bioreactor (ADMET, Norwood Massachusetts, USA) that measure forces between 1 mN to 5 N at 1.2 mm/s, but does not have a quick clamping system for soft biological materials. Other industrial testers such as an Instron®

universal testing machine can be used, but a large specimen must be made to obtain readings. Thrombin added to fibrinogen and cross-linked with FXIII were used in a casting of 4 mm diameter x 60 mm long, and the measured forces were as high as 0.8 N with an extension of two times the normal length [2]. Soft biological materials may not always be large, so a smaller specimen scale solution is necessary.

Some tensile testers are created for very specific tests. Jacquet et al. created an extensometer to test the mechanical properties of skin on human subjects [40]. The device used a linear variable displacement transducer (LVDT) and strain gauges to measure skin displacement. Krone et al. bonded a hydrogel to silicon, allowing clamps to directly hold the composite specimen to be pulled apart with a Futek load cell [41]. Krasokha et al. casted porcine blood in an aluminum mold, and then aged the clots for 48 hours to be pulled apart horizontally with their tensile tester [4]. However, the data drawn from the tensile testing did not comprise of a continuous data set and had two distinct different linear slopes in the stress vs. elongation plots. A contributing factor may have been that aged clots were more brittle. Tensile testing proved to be possible on blood clots, but the data were not as refined as other methods such as AFM or rheometry, possibly due to the difficulty of pulling on blood clots.

2.2.5 Electrowetting-On-Dielectric

Electrowetting-on-dielectric (EWOD) is a principle in digital microfluidic devices that uses electrostatic forces to move a liquid on a specialized hydrophobic platform. The platform has a set of activation pads that turn a voltage on and off to move the fluid around the device [42], [43]. EWOD platforms can be used to test clots, since the device

can activate separate pads to pull the specimen apart or move to the desired location. The device is has fine enough resolution to create 900 nL cross-linked alginate specimen on the platform [44]. The placement of calcium chloride relative to the sodium alginate is important, because irregular shaped gels can be formed due to the cross-linking reaction time. A uniform gel was created by moving the calcium to the alginate, so the excess liquid could easily be removed after gel formation [44]. The EWOD platform is promising as an emerging technology, but the blood viscosity and clot strength may be difficult to overcome.

2.3 Specimen Holding Methods

Holding methods vary from apparatus to apparatus as indicated earlier. The main methodologies are through compression, clamping, and special adhesion coatings. Rheometry does not require special holding methods, because the volume is controlled by the rotating compression disk. Krashoka et al. relied on the chamber dimensions and plate to keep the specimen in place [4]. Murphy et al. was able to cast samples into a prescribed shape when platens were used to compress the specimen [36].

A variety of methods and test shapes have been used for tensile testing. Typically all of the hardware used for holding clots or clot-like specimens are simplistic flat clamps with screws to adjust the clamping force. The clamping methodology is possible if the specimen is large and structurally strong enough to withstand outside forces. Brown et al. created a specimen that was 4 mm diameter cylinder x 60 mm long cast of fibrinogen, thrombin, and FXIII mixture [2]. The specimen retained its shape and was held together with a rubber clamp for tensile testing. Krone et al. had a different approach by using a

thin film bonded with a hydrogel, using a bonded bi-layer to characterize the mechanical response via strain energy functions [41]. The method factored out the contributing mechanical role of silicon to obtain the mechanical properties of only the hydrogel.

Chemical adhesion techniques have also been used to secure a specimen on to glass slides for pull testing. In order to promote adhesion of fibrin to glass substrates, surfaces were pretreated with fibrinogen as in [45]. Fibrin can also attach to glass sides via poly-l-lysine (PLL) coating mixed with fibrinogen, which has a net negative charge at pH 7.4 allowing for a bond based on polarity [46]. Adhikari et al. used a peripheral venous catheter tube to create fibrin specimens in 0.8 mm x 5 cm which were able to retain the shape even after being removed with a syringe to be placed on glass slides using cyanoacrylate adhesive [18]. A collagen adhesion method uses collagen directly on slides, allowing time for gelling to promote adhesion [47]. Alginate can adhere to slides with PLL and then barium chloride, under which conditions the PLL, will bind to the prostate-specific membrane antigen on one side and alginate will adhere to the other side [47].

3. THEORY

Three applications of mechanical engineering theory are presented in this chapter: (1) stiffness compensation for inline sensing, (2) nonlinear material stiffness, and (3) lumped parameter modeling of viscoelasticity.

3.1 Stiffness Compensation for Sensing

The ability of a cantilever-type load cell to measure small forces is partially attributed to the load cell's relatively large compliance (compared to a button or s-beam load cell, for example). Placing the load cell in series is advantageous because the load cell cannot be overloaded. Once the specimen tears, the actuator is no longer coupled to the load cell.

As the actuator applies displacement, however, the mechanical response of the system as measured by the load cell includes a mechanical response of the test specimen as well as the stiffness of the load cell body. Figure 1 illustrates the mechanical coupling arrangement.

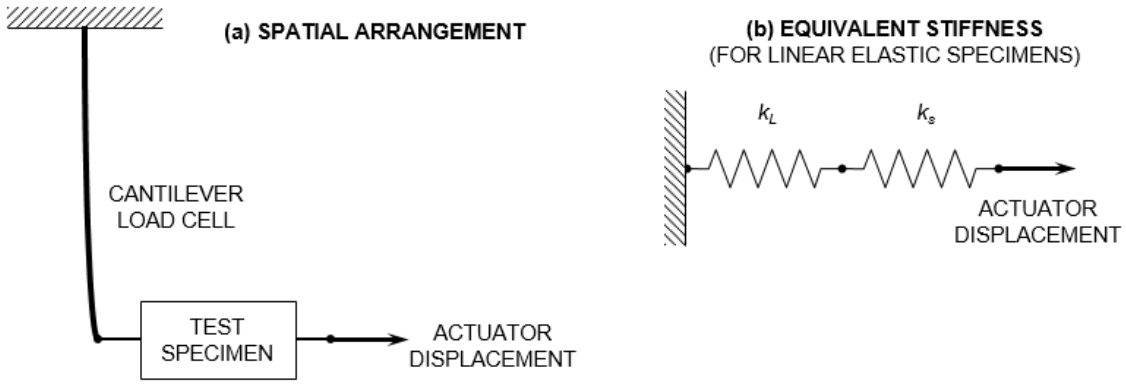

Figure 1. Mechanical coupling from actuator through specimen to load cell, as arranged spatially (a) and as equivalent stiffness elements (b).

Thus, in order to isolate specimen mechanics, both the displacement and the stiffness contributions must be decoupled. The elongation δ_s of the specimen is the displacement δ_{total} of the actuator minus the tip deflection δ_L of the load cell. The tip deflection of the load cell can be measured in real time under a microscope or characterized prior to experimentation based on the measured stiffness k_L (i.e., by applying a known load, measuring tip deflection, and fitting a line to the slope). The stiffness of the load cell can also be estimated by a cantilever beam equation using Young's modulus (if known) and geometric dimensions, although measurement using known weights is more direct and accurate.

When considering only the instantaneous stiffness of the specimen (i.e., not including viscous effects), the load cell stiffness k_L and the specimen stiffness k_s have an equivalent stiffness k_{eq} as shown in equation (1).

$$k_{eq} = \frac{k_L k_s}{k_L + k_s} \tag{1}$$

In quasi-static tensile testing, the force F throughout the series assembly is constant, and the ratio of measured force to actuator total displacement provides the equivalent stiffness, such that the measured force and applied displacement are related to specimen stiffness as shown in equation (2).

$$\frac{F}{\delta_{total}} = \frac{k_L k_s}{k_L + k_s} \tag{2}$$

Rearranging equation (2) provides an expression for the specimen stiffness in terms of the measured force, applied displacement, and (separately characterized) load cell stiffness, as shown in equation (3).

$$k_s = \frac{k_L F/\delta_{total}}{k_L - F/\delta_{total}} \tag{3}$$

3.2 Nonlinear Material Stiffness

Broad categories of material models include linear elastic, nonlinear elastic (hyperelastic, for example), and viscoelastic, all of which can be characterized by uniaxial testing. For mechanical testing, linear elastic materials are conventionally characterized solely by tensile or compressive Young's modulus E. Poisson's ratio ν is also an important linear elastic parameter, but for small test specimens the value is not typically measured and reported.

Three common ways of describing geometric change for uniaxial tensile test specimens are elongation δ, axial strain ε, and stretch ratio λ. Elongation δ, of a loaded specimen is defined as difference between the specimen length L (in its loaded state) and its original length L_o. Axial strain ε is the component of displacement gradient along the axial direction, and for discrete measurements can be expressed as the ratio of elongation to original length. Stretch ratio λ is commonly used in strain energy functions for hyperelastic material models, and is defined as the ratio of the specimen length L when loaded and its original length L_o when not subject to a load. In this study, Cauchy stress, also known as true stress, will be reported in this thesis. Cauchy stress differs from engineering stress (which assumes a constant area) by accounting for the change in the

specimen cross-sectional area throughout the pull testing. Cauchy stress is more completely described as a tensor σ, but for uniaxial tension only the normal component σ_{11} along the direction of stretch is considered (for which the "11" subscript will subsequently be omitted).

A convenient way to evaluate the strain stiffening properties of the blood clot is with a hyperelastic model. Even though blood is a biological material, blood still exhibits elastic qualities because the material will retract when released after extension. Although complex materials are strain-rate dependent, many soft tissues are known to be "pseudoelastic" (i.e., relatively independent of strain rate) [48] and strain-rate sensitivity is not examined in this thesis. There are several hyperelastic material models that have been investigated for soft tissue biomechanics. Neo-Hookean and Mooney-Rivlin models are typically used to describe rubbers, but blood clots have similar elastic deformation properties [49], [50]. Constitutive models are based on strain energy density functions, for which a set of constitutive parameters are typically fit to experimental data under specified loading conditions (e.g., uniaxial, biaxial, or shear) in order to quantify material behavior [51]. Equation 4 will be used as a two-parameter Mooney-Rivlin model [50] to create a responsive fit for blood clots in this study, and the hyperelastic parameters C_1 and C_2 will be extracted from experimental data. However, the Mooney-Rivlin model will not have an accurate viscoelastic model with only uniaxial testing, because pure shear and equibiaxial testing are needed for a complete viscoelastic model [52].

$$\sigma = 2(\lambda^2 - \frac{1}{\lambda})(C_1 - \frac{C_2}{\lambda}) \tag{4}$$

3.3 Lumped Parameter Modeling of Viscoelasticity

Connective tissues have been shown to exhibit both linear elastic and viscoelastic behavior under tension [53]. The Maxwell model is comprised of one spring and one damper in series and is useful for describing stress relaxation under a prescribed displacement. The Kelvin-Voigt model is comprised of one spring and one damper in parallel, and is useful for describing creep under a prescribed load. A three-parameter viscoelastic model commonly known as a "standard linear model" (occasionally referred to as a Kelvin body [54] or a Zener model [15]) uses a spring and damper in series arranged in parallel with another spring. This model captures both stress relaxation and creep phenomena that the Maxwell and Kelvin-Voigt model represent independently. An expanded version of the standard linear model is known as the generalized Maxwell model, which is a standard linear model in parallel with many Maxwell models which allows for more control in the model. van Kempen performed a rheological test on clots with different platelet concentrations contracting on fibrin networks and used a modified generalized Maxwell approximation to extract time-dependent, nonlinear viscoelastic properties to verify against other rheological approaches [55]. Schmitt et al. characterized animal blood by utilizing several models – Maxwell, Kelvin-Voigt, Jeffrey, Zener, and generalized Maxwell. The most appealing of the models is the Zener model, which is comprised of both the Maxwell and Kelvin-Voigt models, by being able to predict stress relaxation along with creep. Schmitt et al. found that more parameters, such as the generalized Maxwell, did not guarantee a better fit when characterizing blood clot dynamics [15].

The lumped parameter used in this thesis is shown in Figure 2, consisting of a three-parameter model with two springs and one damper, assembled in series with an additional spring element to account for stiffness of the load cell. This configuration was chosen because the load cell displacement is not trivial and would contribute to smaller k_1, k_2, and η parameters by approximately 10%. Compensation for the load cell stiffness thus provides a more accurate representation of specimen stiffness.

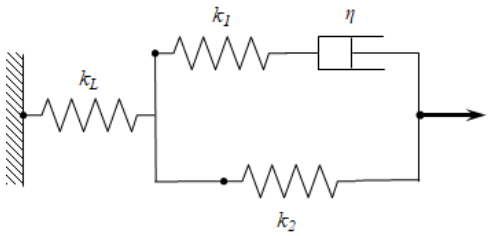

Figure 2. Lumped parameter model, with k_2 as a spring in parallel to spring k_1, and damper η in series added to loadcell k_L.

The differential equation for the standard linear model (without k_L in Figure 2) is shown in equation 5, where F is time-varying force and δ_s is the elongation of the tested specimen.

$$F(t) + \frac{\eta}{k_1}\dot{F}(t) = k_2(\delta_s(t) + \frac{\eta}{k_2}(1 + \frac{k_2}{k_1})\dot{\delta}_s(t)) \tag{5}$$

In the case of stress relaxation, the imposed elongation remains constant such that its time derivative is zero for time $t > 0$. Substituting a time constant $\tau = \eta/k_1$ leads to the differential equation in a single variable $F(t)$.

$$\delta_s = \frac{F(t) + \tau\dot{F}(t)}{k_2} \tag{6}$$

The Laplace transform with parameter s results in equation 7.

$$\frac{\delta_s}{s} = \frac{F(s) + \tau F(s)s - \tau F(0)}{k_2} \tag{7}$$

Solving this differential equation with initial condition of $F(0) = k_1\delta_s + k_2\delta_s$ results in equation 8 as the solution for elongation in the specimen as a function of time.

$$\frac{\delta_s}{s} = \frac{F(s) + \tau F(s)s - \tau(k_1\delta_s + k_2\delta_s)}{k_2} \tag{8}$$

The force is then decoupled on the left in equation 9 to perform an inverse Laplace transform.

$$F(s) = \delta_s\left(\frac{k_2}{s(s\tau + 1)} + \frac{\tau(k_1 + k_2)}{s\tau + 1}\right) \tag{9}$$

After the inverse Laplace transform, equation 10 presents the force-time relationship for the standard linear model without the load cell.

$$F(t) = \delta_s(k_2 + k_1 e^{-t/\tau}) \tag{10}$$

Adding a load cell in series with the standard linear model results in equation 11, where the total observed displacement δ_{total} accounts for elongation of the specimen as well as deflection of the cantilever load cell. Larger forces and a faster displacement will be seen in the stress relaxation portion of the experiment, thus the load cell spring stiffness is included in the equation.

$$F(t) = \frac{\delta_{total} k_L(k_2 + k_1 e^{-t/\tau})}{k_L + k_2 + k_1 e^{-t/\tau}} \tag{11}$$

Equation 11 will be the equation used to fit a curve to the experimental data. MATLAB (The MathWorks, Inc., Natick, Massachusetts, USA) has a nonlinear least squares fit function that uses the three variable inputs k_1, k_2, and η. The function minimizes the residual errors between the data sets and requires an initial guess. Both of the MATLAB Newton step-based solvers "trust-region reflective" and "Levenberg-

Marquardt", yielded the same C_1 and C_2 parameter values in the Mooney-Rivlin equation seen in equation 4.

4. METHODOLOGY

4.1 Device Design

The apparatus for tensile testing consists of a motorized nanopositioner (MP-285, Sutter Instrument, Novato, CA), a full-bridge thin cantilever load cell (LCL Series, OMEGA Engineering, Norwalk, CT), and a data acquisition (DAQ) signal conditioner DI-1000U (Loadstar Sensors, Fremont, CA). The specimen is placed between the actuator and load cell using magnetic clamps, as shown in Figure 3.

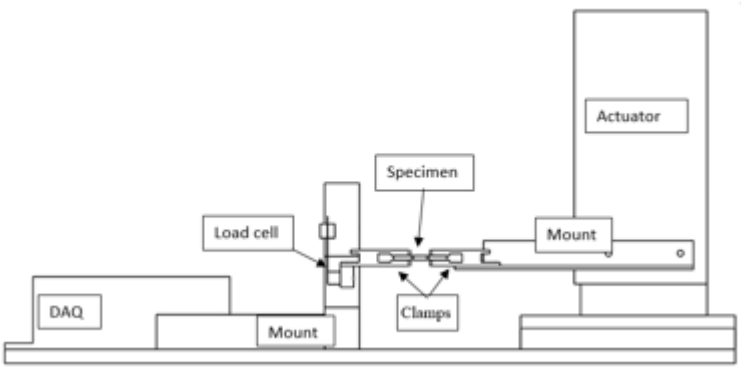

Figure 3. Major component of tensometer system.

The nanopositioner has 25 mm range with fine resolution of 40 nm per step. Speeds are selectable from 20 µm/s to 2.9 mm/s. The data reported in this paper was recorded using the 113 g capacity load cell from the LCL product series, but load cells are interchangeable with higher-load products of the same family (e.g., 227 g, 454 g, 816 g). The DI-1000U DAQ has 24-bit resolution (over 16 million levels) and up to 80 Hz sampling rate.

The test specimen is mechanically in series with the load cell, offering a fail-safe design such that the specimen would always tear before the actuator can deflect the load

cell beyond its designed range of operation. However, this series arrangement requires that the tip deflection of the load cell be subtracted from the raw displacement of the actuator, in order to determine the net elongation of the test specimen.

4.1.1 Functional Requirements

Mechanical properties of biomaterials are difficult to characterize experimentally because many relevant biomaterials such as hydrogel, collagen, and fibrin are pliable and viscoelastic. Furthermore, test specimens for substances such as blood clots tend to be small in size (i.e., on the order of a few millimeters), requiring fine-resolution positioning (i.e., submicron) and sensitive force measurement. Mechanobiological studies further require high frequency data recording (i.e., faster than 10 Hz), preferably under simultaneous microscope imaging, in order to monitor events such as structural remodeling or localized rupture while strain is being applied. A low-profile tensile tester that applies prescribed displacement up to several millimeters and measures forces with resolution on the order of millinewtons has been designed and tested.

4.1.2 Specimen Clamping Method

Clamping has been the most successful methodology for pulling soft biomaterial test specimens with tensile testing. An aluminum clamp with a toothed crevice as seen in Figure 4 allows for two points of contact to hold the test specimen. A magnet was press fitted inside the clamp bottom to create a clamping force with the top clamp that has a steel screw attached. The magnetic clamping force can be readjusted by turning the screw to the desired height and locking the screw in place with the appropriate nut. An

adjustable force allows for the clamps to compensate for different sized specimens and unwanted damage to the specimens.

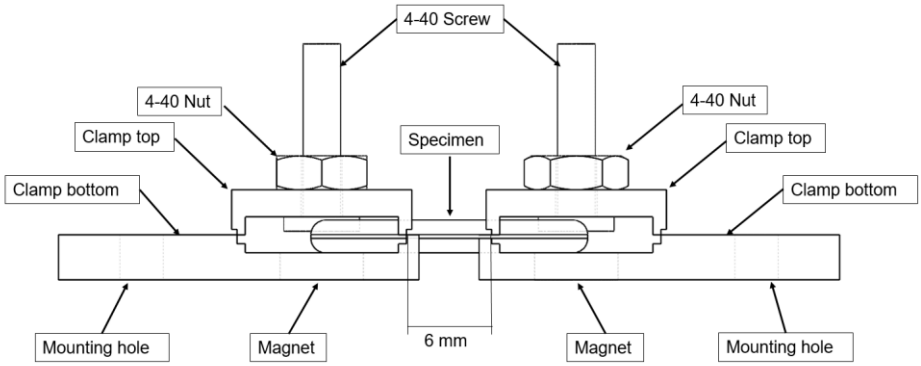

Figure 4. Adjustable magnetic clamps used to hold the specimen.

4.1.3 Displacement Measurement

The load cell was calibrated using three known weights of 10.950 g, 20.947 g, and 51.248 g, as measured by a precision balance (Sartorius Research, Gottingen, Germany). By adjusting the mN/mV calibration factor, the calibration error was limited to 1% for loads up to 508 mN. The rated capacity of the load cell was 1.1 N, which is well above the specimens maximum tested force of 300 mN.

Stiffness of the load cell was determined by applying known weights and measuring the corresponding cantilever displacement with an optical comparator (HB400, Starrett, Athol, MA). The comparator has a resolution of 2.5 μm at 10X magnification. The load cell was placed horizontally in the comparator and a clamp was used to hold the base stationary. Calibration weights of 10.950 g, 20.947 g, and 51.248 g were applied and the corresponding tip deflection was measured using the optical comparator. As shown by the force vs. displacement data in Figure 5, the cantilever load cell had a stiffness of k_L =

96.883 N/m. The corresponding R^2 value of 0.9985 with respect to straight-line fit indicates a highly linear behavior of the cantilever.

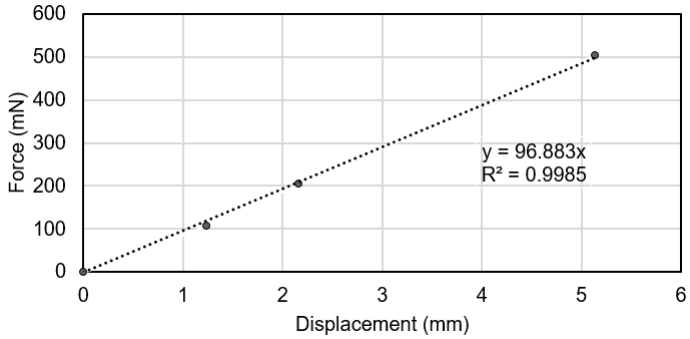

Figure 5. Cantilever load cell stiffness.

Figure 6 shows a representative plot of the zero-load offset and noise of the load cell. The signal standard deviation over a 300 s period was 48 µN. The plot shows a mean offset of 50 µN and a root mean square (RMS) variation of 68 µN. Typical specimen tests are on the order of 100 mN, such that the signal-to-noise ratio is very high. These measurements are consistent with manufacturer rating of ± 0.02% accuracy.

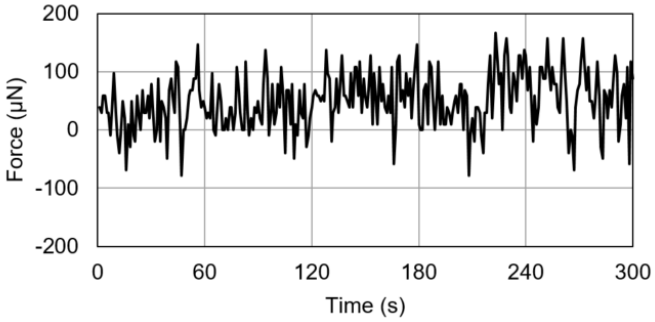

Figure 6. Zero-load offset and noise for the load cell.

Zero-load return behavior of the load cell was inspected by repeatedly applying and releasing manual load up to 200 mN by pushing with a mechanical micromanipulator. The load cell returned to zero (within the previously determined mean offset of 50 µN) after each cycle, as evidenced in Figure 7.

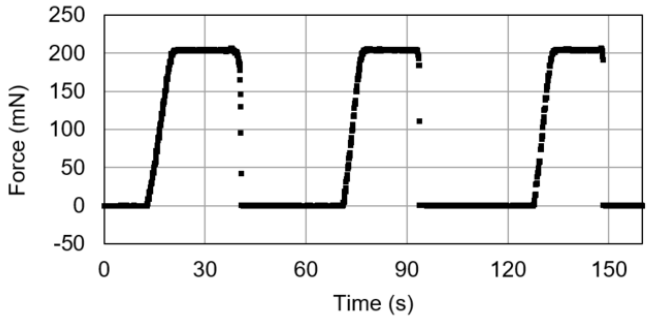

Figure 7. Zero-load return upon applying and releasing manual loading cycles.

4.2 Experimentation

4.2.1 Experimental Design

Test were conducted at room temperature. The blood draw was compliant with the approved F16134 San Jose States Institutional Review Board (IRB) protocol. Five different donors were used for the test. Calcium is removed during the blood draw to prevent unwanted clotting from initiating and is accordingly reintroduced before pull tests to restore the blood to its more natural composition. Four different treatments were tested with whole blood as the control, blebbistatin for the myosin II inhibitor, cytochalasin D for the actin inhibitor, and the combination of blebbistatin plus cytochalasin for observation of combined effect.

The human blood specimens were fabricated and tested within a 4 hour period after the blood was drawn for each treatment. Four specimens were made in each well on a chamber slide (Nunc Lab-Tek, Thermo Scientific, Waltham, MA). The tests were conducted with two or three successful pulls for each treatment. The order of testing and fabrication was whole blood, blebbistatin, blebbistatin plus cytochalasin, and then cytochalasin. Between each treatment there was a 30 minute time window to test each set of four specimens to complete all of the testing within 4 hours of the blood draw. The

whole blood was created first, the blebbistatin incubation mix was started immediately after, the blebbistatin plus cytochalasin mix started 30 minutes after the blebbistatin, and finally the cytochalasin incubation was started 30 minutes after the blebbistatin plus cytochalasin mix to perform all of the test within the 4 hour time period.

The actuator was set to move at a prescribed rate of 100 μm/s for 3 mm and then 400 μm/s for 1 mm subsequent increments with approximately 30 s of relaxation between each increment until a set distance of 6 mm was reached. A mechanical dial indicator was attached to an adjustable mount to verify the distance traveled by the actuator and to corroborate the digitally displayed on the MP-285 actuator.

4.2.2 Specimen Fabrication

The dispensing of the blood was performed under a biological safety hood (SG303, The Baker Company, Sanford ME). 500 μL specimens were cast into a chamber slide with dimensions of 11 mm x 19.5 mm x 11.25 mm to obtain a consistent rectangular starting shape. The estimated starting size of all clots prior to retraction was 11 mm x 19.5 mm x 2.3 mm. All blood clots were given 1.5 hours to retract and to stabilize in a relaxed state such that contraction forces would not interfere with results. The retraction of each specimen varied and thus required a microscope and a side camera to measure the specimen to calculate the actual dimensions, because inconsistent image analysis can adversely affect the results of the study [56].

The whole blood control treatment consisted of 0.3 U of thrombin (Thermo Fisher Scientific, Waltham, MA) to initiate the clot, 10 μM of calcium chloride (Thermo Fisher Scientific, Waltham, MA) to replace the calcium initially removed during blood draw,

and 600 µL of blood to mix everything together. After mixing the clot three times (moving the fluid up and down) in the pipette for 5 s, 500 µL of the blood mixture was dispensed into the specimen well and the clot was allowed to retract and stabilize for 1.5 hours in the biological safety hood.

The other three treatments blebbistatin (Thermo Fisher Scientific, Waltham, MA), blebbistatin plus cytochalasin mix, and cytochalasin (Thermo Fisher Scientific, Waltham, MA) were incubated at room temperature (23 °C) for 30 minutes on a lab rocker (Vari-Mix Platform Rocker, Thermo Fisher Scientific, Waltham, MA) at approximately 2 Hz with eppendorf tube secured horizontally to improve mixing with the whole blood. Table 1 shows the concentrations used for the experiment. The blebbistatin and cytochalasin concentration values were higher than in other reported studies [35] to prevent contraction of the clot, by completely inhibiting the desired mechanism. The blebbistatin treatment had 300 µM of blebbistatin mixed with 600 µL of blood, the cytochalasin treatment had 10 µM of cytochalasin mixed with 600 µL of blood, and the combined blebbistatin plus cytochalasin had 300 µM of blebbistatin, 10 µM cytochalasin, and 600 µL of blood. All three treatments had 0.3 U of thrombin and 20 µM of calcium added after the incubation period and were mixed within approximately 5 s in a pipette three times prior to dispensing 500 µL of the treated blood into the specimen wells. All specimens were left in the biological safety hood for 1.5 hours to complete retraction.

Table 1. Composition and timing used for each specimen type

	Blebbistatin	Cytochalasin	Blood	Incubation	$CaCl_2$	Thrombin	Relaxation
Whole Blood	0	0	600 µL	N/A	20 µM	0.3 U	1.5 hours
Blebbistatin	300 µM	0	600 µL	0.5 hrs	20 µM	0.3 U	1.5 hours
Cytochalasin	0	10 µM	600 µL	0.5 hrs	20 µM	0.3 U	1.5 hours
Blebbistatin + Cytochalasin	300 µM	10 µM	600 µL	0.5 hrs	20 µM	0.3 U	1.5 hours

4.2.3 Apparatus and Measurement System

The nanopositioner started at its left-most position to utilize the entire travel of the motor. The clamps were placed on the actuator and the load cell mount. The load cell and its corresponding clamp were attached on a micromanipulator (Cascade Microtech, Beaverton, OR), initially set flush with the opposing clamp on the actuator. Another micromanipulator with a dial indicator was set to zero prior on the load cell micromanipulator. The load cell clamp was then moved away from the actuator clamp until 4.24 mm on the dial indicator is read for total of 6 mm initial working distance (each clamp has a channel width of 0.88 mm). The dial indicator was moved perpendicular to the actuator and zeroed to verify the distances the actuator moved.

The test data were extracted in terms of force and converted to the respective true stress vs. stretch ratio curves and stress relaxation curves. A specimen was continuously pulled to 3 mm at 100 µm/s which was 50% of the initial 6 mm working length to obtain the true stress vs. stretch ratio data. The specimen was allowed to rest for 30 s between each increment. All subsequent increments added additional 1 mm extend-and-hold operations, moving at 400 µm/s. At the end of the test, a total specimen length of 12 mm was reached at 100% specimen elongation.

The load cell was zeroed without the bottom support to neglect the weight of the specimen in the initial pull. Prior to pulling, the microscope was set to capture top-view images of the specimen to extract top cross-sectional dimensions, and the side camera was used to side-view images to extract thickness. The microscope captured three images during the pull, each 8 s apart. The force recording from the data acquisition software (LoadVUE, Loadstar Sensors, Fremont, CA) and actuation of the nanopositioner were started simultaneously and force measurements were recorded at 30 Hz. The actuator was controlled by legacy software "mp285.exe" provided by the nanopositioner manufacturer (Sutter Instrument Company, Novato, CA), and followed the sequence stated earlier. As soon as the first actuation stage completed, the second specimen side view picture was taken prior to the 30 second timer starting for the stress relaxation pulls. The pull timing allowed for 3 s of travel. After, every 30 s the next actuation stage was enabled. The times were 30 s, 1 minute 3 s, 1 minute 36 s, 2 minutes 9 s, and 2 minutes 42 s. The entire pull portion of the experiment took 3 minutes 12 s to complete.

4.2.4 Image Analysis

The image analysis tool Fiji was used to measure the three top-view images for the width w and two side images for thickness t [57]. Figure 8 show a typical set of images that were captured during the true stress vs. stretch ratio portion of the experiment from the top view. Each image was used to understand the changing cross-section of the specimen. The 12.7 mm clamp width was a reference feature used to measure the clot width at the center of the specimen in each image. A fitted line from each of the three images was used to estimate the change in width and thereby to determine the cross-

sectional area of the specimen. Force measured by the load cell was divided by cross-sectional area to calculate true stress.

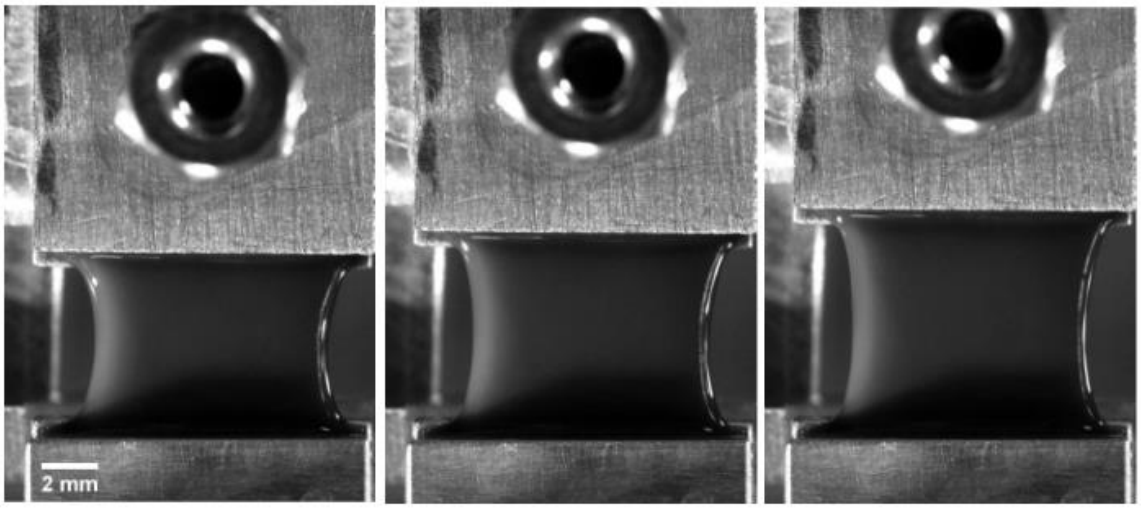

Figure 8. Standard top down three images at 8 s apart for each specimen.

Figure 9 shows the two images taken on the side to measure the change in thickness over time for the true stress vs. stretch ratio portion of the experiment. The 3 mm clamp thickness was used as a reference feature to calculate the for clot thickness at the center of the specimen. A straight line drawn across the center was used to measure the specimen thickness change. The specimen cross-section was not quite rectangular, but closer to an elliptical profile with rounded edges. Equation 12 used the width and thickness founded to calculate the true stress with the changing area as an ellipse.

$$A = \frac{\pi w t}{4} \tag{12}$$

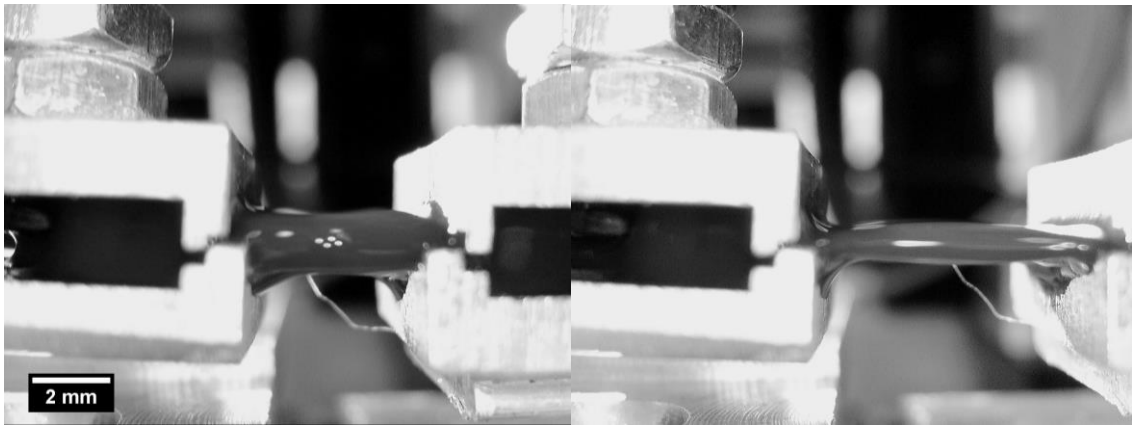

Figure 9. Side view of specimen being pulled from initial (left) to 3 mm extension (right).

4.2.5 Data Analysis

Figure 10 shows a representative example of raw data plot from the test. The first portion of data was used to plot true stress vs. stretch ratio. The first stress relaxation curve (in the 30 s to 60 s time frame) following the initial pull was discarded so that each step change for stress relaxation could be applied in a consistent manner. The next three pulls was used for the stress relaxation portion of the study.

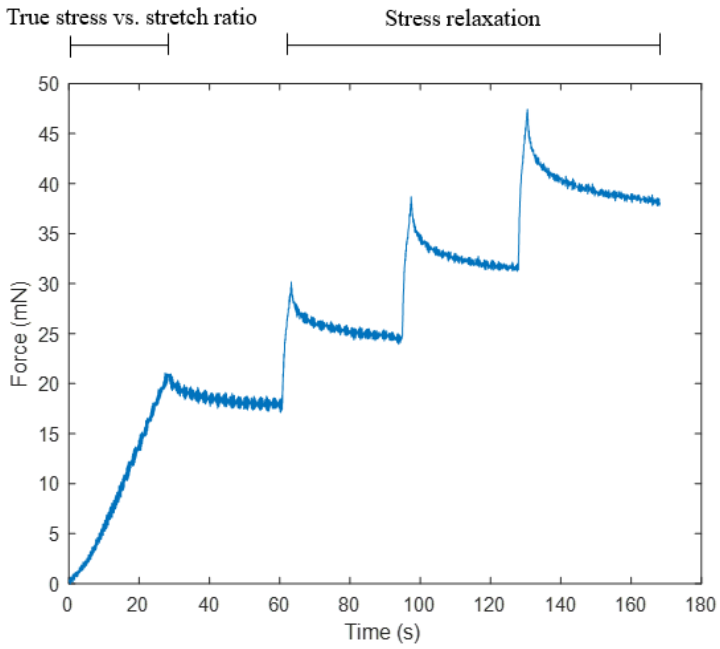

Figure 10. Representative extension curve to extract true stress vs. stretch ratio plots and stress relaxation plots.

The force for the strain stiffening portion of the test reached a maximum of 3.5 g which was a factor of 10 less than the load cell operating range of up to 113 g. Force was divided by the changing area to provide the true stress of the specimen. The time output was converted to a stretch ratio with the known displacement rate and initial specimen length. Mooney-Rivlin fit parameters can be extracted from the plots.

The first three seconds of each relaxation curve was analyzed by fitting the experimental data to equation 11. Figure 11 shows a sample plot of the three pull distances overlaid with the fitted equation 11 used to extract parameters k_1, k_2, and η. The important parameter k_1 and η make up the time constant $\tau = \eta/k_1$, because k_2 only shifts the height of the plot and does not play a role in how fast the curve decreases.

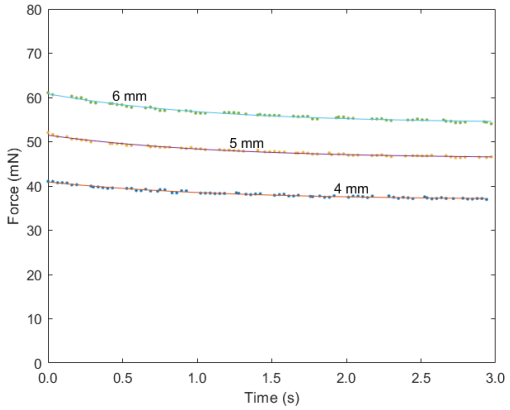

Figure 11. A consolidated fitted curve plot at the 4 mm, 5 mm, and 6 mm on the first 3 s of the specimen pulls.

To determine donor-to-donor variability the Mooney-Rivlin parameters was used in a one way analysis of variance (ANOVA) at a 99% confidence interval (α = .01) based on whole blood specimens only. C_1 and C_2 each had an independent ANOVA performed, because the values are dependent on each other. Each parameter will need to have a high p-value for all the donors to be equal. The differences between the maximum and minimum C_1 and C_2 values within each donor provides the within donor variability information.

4.3 Sources of Uncertainty

In the test calibration, a 10.950 g weight displayed an average force output of 108.54 mN resulting in a 1.05% error from the theoretical force 107.42 mN, the 20.95 g weight displayed an average force output of 207.29 mN resulting in 0.86% error from the theoretical force 205.52 mN, and 51.250 g weight measured 508.16 mN, resulting in a 1.07% error from the theoretical force 502.76 mN. The scale used to measure the weights had a resolution of 0.1 mg.

Actuator speeds were verified against the program values. The speed was checked

against the distance. A 12.7 mm depth gauge was attached on the actuator to verify distance traveled for the two prescribed rates of 20 µm/s and 60 µm/s. The actuator was programmed to move 2.54 mm at the rates of 20 µm/s and 60 µm/s, and a stopwatch verified the times to be 127 s and 42.3 s, respectfully. The dial has a resolution of 25.4 µm and the estimated average human reaction time is roughly 0.25 s.

The stiffness of the load cell calculation will vary on many parameters, because all of the measurements will affect the length and cross-sectional values used to determine the stiffness value. The length, width, and thickness were measured with a micrometer with a resolution of 2.5 µm. The load cell deflection was measured on an optical comparator by putting the load cell flat lengthwise to allow for known weights to be added at the end. A zero reference was created with the unloaded load cell. Weights were added the static system and then measured by a comparator with an uncertainty of ± 2.5 µm. In the image analysis there was a pixel uncertainty of approximately ± 10 µm. Table 2 is a summarized list of uncertainties that was used to calculate apparatus uncertainties in true stress reporting and load cell stiffness.

Table 2. List of uncertainties

Source	Magnitude of uncertainty
Optical comparator	± 2.5 µm
Balance	± 0.1 mg
Image analysis	± 10 µm
Load cell	± 1%

Using the list of uncertainties in Table 2, the apparatus measurement uncertainty was calculated. Applying equation 13, the propagation of uncertainty, a square root sum of squares of uncertainties, is used to estimate the total uncertainty. A combined error *u*, is

characterized by *f* which is the function with the unknown uncertainty with the sources of error. The first source of uncertainty is $y_1$with an uncertainty range defined as u_1.

$$u = \sqrt{\left(\frac{\partial f}{\partial y_1}u_1\right)^2 + \left(\frac{\partial f}{\partial y_2}u_2\right)^2 + \left(\frac{\partial f}{\partial y_3}u_3\right)^2 + \ldots + \left(\frac{\partial f}{\partial y_n}u_n\right)^2} \tag{13}$$

To find the cross-sectional area uncertainty from the image analysis equation 14 is used. The two sources of uncertainty are thickness and width which are both from image analysis tool. All specimens have different cross-sections and a smaller cross-section would result in a larger stress uncertainty in later calculations. The assumed dimensions are 0.85 mm thick x 7.74 mm wide, because those were the smallest measured values for each of their respective features. The combined uncertainties resulted in a cross-sectional uncertainty of 0.06 mm² with the image analysis tool.

$$u_A = \sqrt{\left(\frac{\pi w}{4}u_t\right)^2 + \left(\frac{\pi t}{4}u_w\right)^2} \tag{14}$$

With the result from equation 14, the reported stress uncertainty is calculated with equation 15. By using the load cell uncertainty from Table 2 and the previous area uncertainty an overall stress uncertainty was calculated. The upper range specimen force of 34.3 mN and lower range specimen area of 5.18 mm² is used to calculate a stress uncertainty of 102.63 Pa or 1.55% error for the nonlinear stiffness calculations.

$$u_\sigma = \sqrt{\left(\frac{1}{A}u_F\right)^2 + \left(\frac{-F}{A^2}u_A\right)^2} \tag{15}$$

For equation 16, the load cell stiffness uncertainty, an assumed force of 106.4 mN from the calibration measurement and a deflection of 1.24 mm. An uncertainty of 0.17 N/m was found for the load cell stiffness.

$$u_{kL} = \sqrt{\left(\frac{1}{\delta_L} u_F\right)^2 + \left(\frac{-F}{(\delta_L)^2} u_{\delta L}\right)^2} \tag{16}$$

The apparatus loading style is subjected to sine error due to the vertical orientation of the load cell and the horizontal pulling of the specimen in relation to the load cell. Equation 17 is used to calculate the sine error ε. The clamp distance h from the load cell is 24 mm to the specimen contact and the angle θ was calculated from force deflection with the load cell stiffness. The maximum forces used are 34.3 mN for the nonlinear stiffness and 106.4 mN for the stress relaxation resulting in an error of 0.42 mm and 1.30 mm respectively.

$$\epsilon = hsin(\theta) \tag{17}$$

However, with image analysis, the clamp shift was found to be closer to 0.12 mm at the 34.3 mN pull. The loading of the cantilever was not exactly the same as the specimen being pulled on the clamps, because the mounting adapter could not attach to the weights used for calibration.

5. RESULTS AND DISCUSSION

There are two main types of results from a single pull sequence. The first result is how the inhibitor treatments affect the stiffness of the specimen, as revealed in a plot of true stress vs. stretch ratio. The second result is how the inhibitor treatments affect the stress relaxation of the specimen.

5.1 Effective Nonlinear Stiffness of Blood

Figure 12 shows fitted two-parameter Mooney-Rivlin curves for true stress vs. stretch ratio for each of the treatments, averaged across all donors and specimens. The plot shows that whole blood has the highest stiffness of all the treatments, as expected because the structure has not been altered with any inhibitors. Based off of the maximum true stress found on the plot in Figure 12, cytochalasin decreased clot stiffness by 33.7% and blebbistatin decreased clot stiffness by 37.9%. The blebbistatin plus cytochalasin mix decreased the clot stiffness by 44.8%. The difference between blebbistatin and cytochalasin is 4.3%, and is greater than the 1.55% uncertainty in true stress, as estimated in Section 4.3.

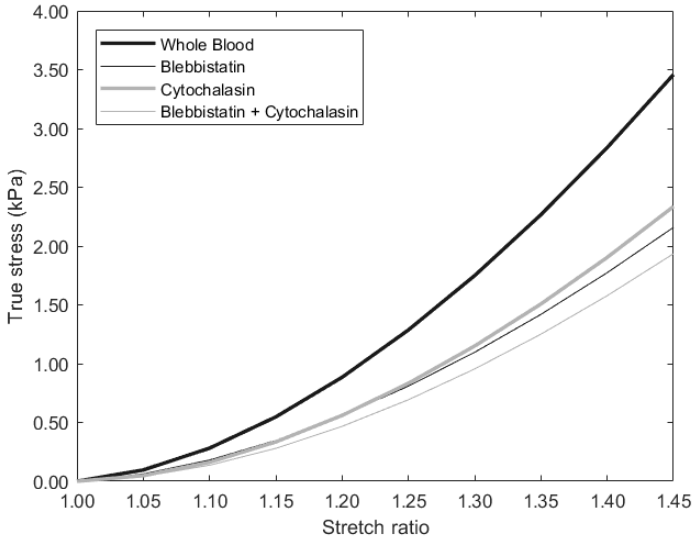

Figure 12. Fitted Mooney-Rivlin hyperelastic model on the averaged treatment results across all donors.

The true stress vs. stretch ratio showed that the whole blood clot was structurally stiffer than the inhibitor-treated clots. Blebbistatin has a lower true stress at maximum stretch ratio than cytochalasin by 4.3%. Although based on limited sample size and fixed concentration, this offers some supports to the hypothesis that blebbistatin affects the blood structure to a greater extent, by preventing the cross-linking of actin filaments through the inhibition of myosin II, thus reducing the overall clot contraction strength. Cytochalasin affects the actin filament length by preventing actin from depolymerization and repolymerization, shortening the myosin II travel distance on the actin. However, the capped actin filaments did not inhibit the myosin II function, causing the cytochalasin treatments to yield stiffer clots. Blebbistatin prevented myosin II function, which created a gap between the actin proteins, because there were no protein cross-linkage interactions. The larger distances between proteins during the pull testing, resulted in a

weaker clot structure, because there was empty space that could easily collapse. The blebbistatin plus cytochalasin combination affected two different mechanisms, which are the myosin II travel on actin filaments and the actin filament polymerization length. The combination of both inhibitors resulted in clots with the lowest overall stiffness.

5.2 Viscoelastic Response of Blood

The bar graph in Figure 13 shows how the time constant τ differs for the four different types of blood clots. A smaller value of τ means rapid decay and implies relative inability to sustain tensile stress. As seen in Figure 13, the fastest τ was observed for the blebbistatin treatment, and whole blood had the slowest time constant at 4 mm extension. At 5 mm extension, the blebbistatin treatment also exhibited the fastest time constant but the cytochalasin treatment showed slower response than whole blood. At 6 mm, the inhibitor mix blebbistatin plus cytochalasin was faster than blebbistatin and cytochalasin was the slowest. The overall data across the three distances imply that blebbistatin, with the fastest time constant, weakens the clot more than cytochalasin. The cytochalasin specimen decay time became slower than whole blood at larger pull distances, which was unexpected.

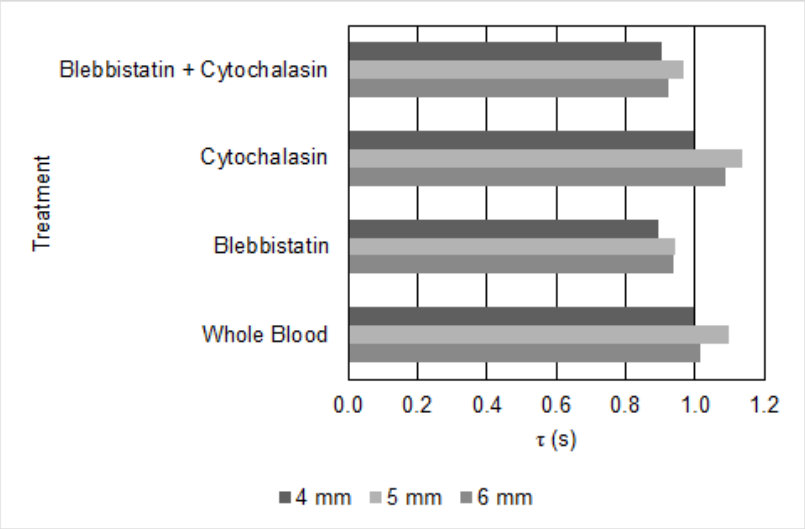

Figure 13. Time constant τ values for each treatment at 4 mm, 5 mm, and 6 mm.

All of the treatments have a similar unexpected trend with slower time constants at 5 mm, but a slightly faster time constant at 6 mm as seen in Table 3. At larger distances, environmental factors such as prolonged air exposure can dry-out the clot and alter the results. Thus, behavior at 6 mm extension is less revealing about changes in clot structure. The time constants at 4 mm extension are considered more accurate, since there are fewer uncontrollable variables in the first pull than in the later pulls. The faster time constants from the stress relaxation exhibit the treatment effects. Blebbistatin has a 10.2% faster time constant than whole blood. The cytochalasin specimen did not differ from whole blood greatly by only being 0.0317% lower.

Table 3. Time constant differences between inhibitor treatments and the whole blood control at each extension distance

	Blebbistatin	Cytochalasin	Blebbistatin + Cytochalasin
4 mm	-10.2%	-0.0317%	-8.86%
5 mm	-14.1%	3.51%	-11.8%
6 mm	-7.73%	6.91%	-9.25%

5.3 Donor Variability

5.3.1 Within-Donor Variability

The variability within donors is shown in Figure 14. Figures 14-1 and 14-2 show specimens in black that are initially weaker than the rest, but see strain stiffening, causing the specimen to reach a higher end stress. The increased strain stiffening resulted in specimen curve in black to intersecting with other specimen curves. Figures 14-2, 14-3, and 14-4 all have a within donor maximum stress difference of 2 kPa at the 1.45 stretch ratio.

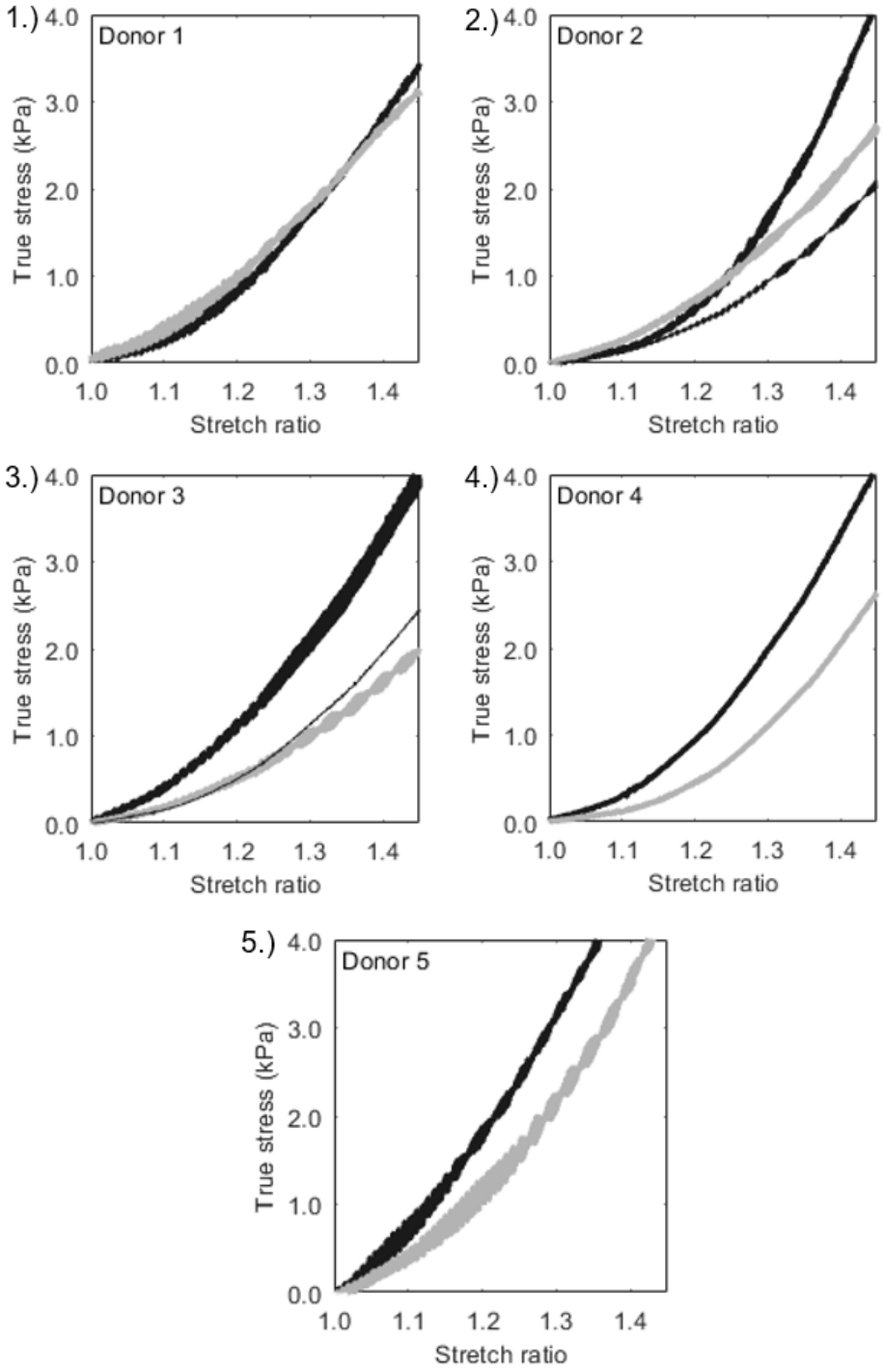

Figure 14. Plots of whole blood donor replicate variability for five donors where each curve is a separate test specimen.

The ranges of fitted Mooney-Rivlin parameters C_1 and C_2 are presented in Table 4, arranged by donor. Donor 2 had the highest variability among the specimens in terms of plot shape, as shown in Figure 14-2, with the largest overall calculated variation of 58% for C_1 and of 62% for C_2. The larger C_2 range compared to the C_1 range correlated with curves intersecting. Each parameter affects the curve, such that C_1 values change the true stress maximum height and C_2 values change the plot curvature shape. Donor 1, 3, and 4 had comparable ranges, but Donor 5 had the smallest difference between values.

Table 4. Whole blood Mooney-Rivlin hyperelastic parameters C_1 and C_2 range for each donor

WB	Donor 1	Donor 2	Donor 3	Donor 4	Donor 5
C1	1.16	3.34	1.67	1.19	0.36
C2	1.56	3.85	1.42	0.93	0.24

5.3.2 Donor-to-Donor Variability

The variability of all treatments across donors was unpredictable with no obvious trend as seen in Figure 15. The whole blood with no treatment across all donors had the highest variability. In Donor 5 the whole blood specimen with highest observed stiffness had maximum true stress that was approximately twice the true stress of the next highest whole blood specimen. The effects of all other treatments were difficult to determine, because they varied between donors. In Donor 1, blebbistatin and cytochalasin are shown with comparable stiffnesses. In Donor 2, cytochalasin appeared to have no effect on the blood. In Donor 3, the results are similar to the averaged Mooney-Rivlin results with whole blood as the stiffest specimen and blebbistatin weaker than cytochalasin. In Donor 4, blebbistatin is the weakest, but in Donor 5 blebbistatin is unexpectedly higher than cytochalasin.

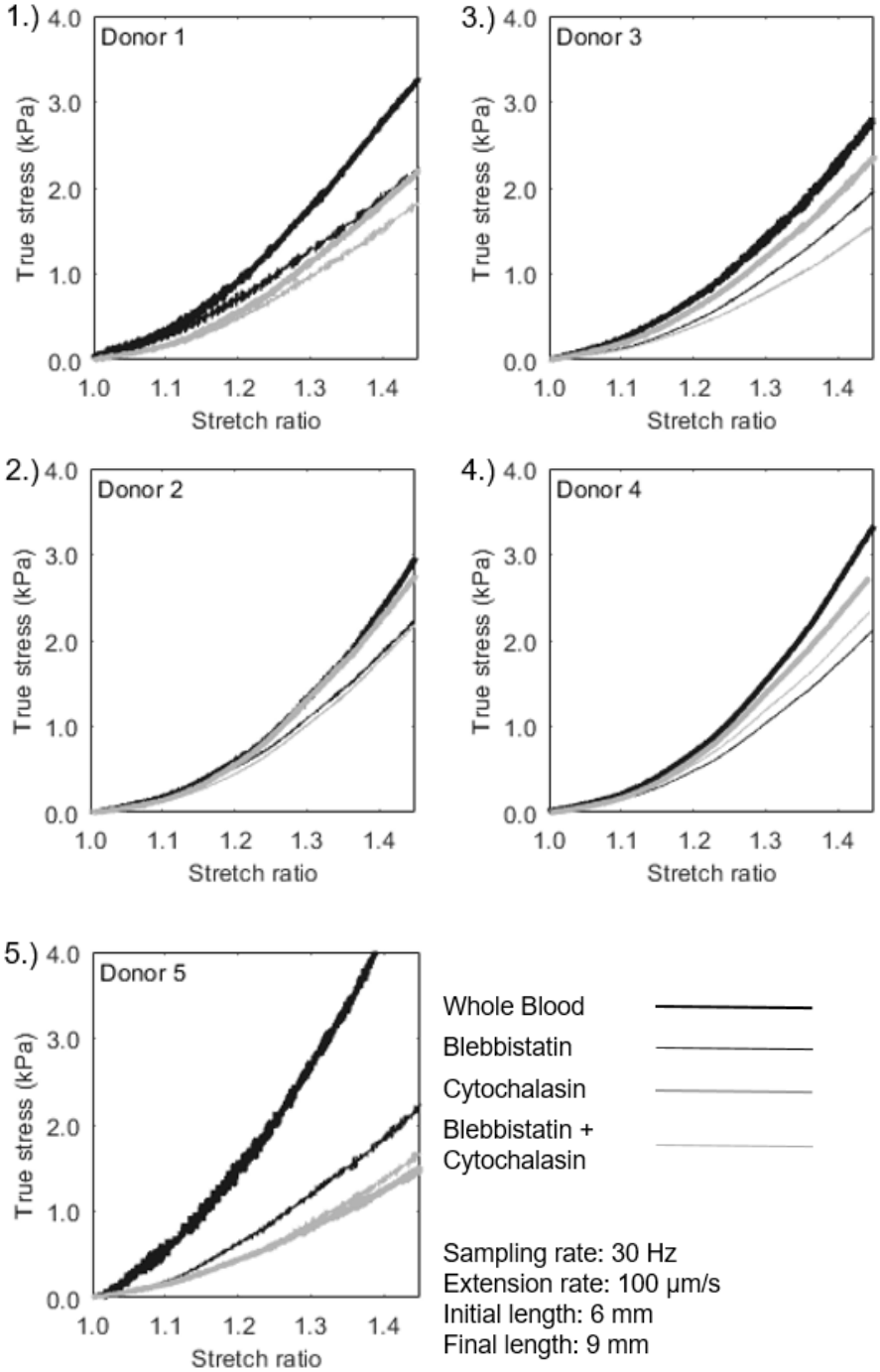

Figure 15. Plots of true stress vs. stretch ratio averaged across five donors per treatment response by each donor.

Analysis of variance (ANOVA) was used to check for statistically significant differences among donors, with each of the two Mooney-Rivlin parameters as separate

response variables, and donor number as the factor of interest. The control whole blood was chosen to determine if there were any difference between the donors and to avoid inhibitor effects on specific donors. Table 5 shows that the C_1 value for five donors had weak evidence of any differences with a p-value of 0.60. Donor 2 showed the highest variance and donor 5 had the lowest variance, similar to the within donor range shown in Figure 14.

Table 5. Mooney-Rivlin parameter C_1 one way ANOVA comparison across donors for whole blood

Groups	*Count*	*Sum*	*Average*	*Variance*		
Donor 1	2	6.27	3.13	0.68		
Donor 2	3	10.74	3.58	3.53		
Donor 3	3	8.46	2.82	0.70		
Donor 4	2	7.87	3.94	0.70		
Donor 5	2	9.06	4.53	0.06		
Source of Variation	*SS*	*df*	*MS*	*F*	*P-value*	*F crit*
Between Groups	4.16	4	1.04	0.74	0.60	4.12
Within Groups	9.90	7	1.41			
Total	14.05	11				

In Table 6, C_2 has a p-value of 0.71, showing weak evidence that the donors are unequal. The high p-value indicates that all the curvatures were similar. Donor 2 showed the highest variance and Donor 5 had the lowest variance which was also shown in Figure 14 whole blood donor plots.

Table 6. Mooney-Rivlin parameter C_2 one way ANOVA comparison across donors for whole blood

Groups	*Count*	*Sum*	*Average*	*Variance*		
Donor 1	2	5.68	2.84	1.22		
Donor 2	3	11.09	3.70	4.87		
Donor 3	3	8.04	2.68	0.54		
Donor 4	2	8.04	4.02	0.44		
Donor 5	2	7.98	3.99	0.03		
Source of Variation	*SS*	*df*	*MS*	*F*	*P-value*	*F crit*
Between Groups	3.91	4	0.98	0.55	0.71	4.12
Within Groups	12.50	7	1.79			
Total	16.42	11				

The ANOVA of the Mooney-Rivlin parameters showed no statistically significant differences with respect to donor for whole blood specimens. Thus the averages from each donor are used for comparing each of inhibitor treatments, even though the composition of specimens from each donor may have had a different platelet and red blood cell count.

The average maximum stress between donors for all treatments for a stretch ratio of 1.45 is shown in Table 7. Whole blood was used as the reference and for each donor there was a shift in the effectiveness of blebbistatin and cytochalasin observed in the plots. In Table 7, whole blood, blebbistatin, and cytochalasin had a donor maximum stress range of 2.23 kPa, 0.29 kPa, and 1.26 kPa respectively. The percentage difference from whole blood ranged from 24.5% to 55.4% for blebbistatin and 6.81% to 69.8% for cytochalasin. The donor-to-donor variability for drug effectiveness had a large range in percentage change.

Table 7. Average maximum stress value percent difference at 1.45 stretch ratio for each treatment with whole blood as the reference

	Maximum Stress				Percent Difference		
	Whole Blood	Blebbistatin	Cytochalasin	Blebbistatin + Cytochalasin	Blebbistatin	Cytochalasin	Blebbistatin + Cytochalasin
Donor 1	3.26 kPa	2.24 kPa	2.20 kPa	1.84 kPa	-31.2%	-32.7%	-43.5%
Donor 2	2.96 kPa	2.23 kPa	2.76 kPa	2.19 kPa	-24.5%	-6.81%	-25.9%
Donor 3	2.81 kPa	1.96 kPa	2.38 kPa	1.56 kPa	-30.3%	-15.6%	-44.6%
Donor 4	3.35 kPa	2.13 kPa	2.71 kPa	2.33 kPa	-36.4%	-19.0%	-30.4%
Donor 5	5.04 kPa	2.25 kPa	1.52 kPa	1.69 kPa	-55.4%	-69.8%	-66.5%

The time constants also varied from donor-to-donor shown in Table 8. For all donors except Donor 3, the treatment time constants at 4 mm were slower than whole blood time constant. In all donors, at 4 mm, the blebbistatin treatment time constants were faster than the cytochalasin treatment time constants. Whole blood, blebbistatin, and cytochalasin had a time constant range between donors of 0.22 s, 0.25 s, and 0.21 s respectively. The time constant ranges varied by no more than 24% within any given treatment type.

Table 8. Average τ value percent difference at 4 mm with whole blood as the reference

	Time Constant				Percent Difference		
	Whole Blood	Blebbistatin	Cytochalasin	Blebbistatin + Cytochalasin	Blebbistatin	Cytochalasin	Blebbistatin + Cytochalasin
Donor 1	1.10 s	0.932 s	0.986 s	0.974 s	-15.5%	-10.6%	-11.6%
Donor 2	1.03 s	0.838 s	0.941 s	0.869 s	-18.5%	-8.43%	-15.4%
Donor 3	0.924 s	1.02 s	1.04 s	1.02 s	10.4%	12.3%	9.91%
Donor 4	1.03 s	0.950 s	1.09 s	0.911 s	-7.76%	5.96%	-11.6%
Donor 5	0.881 s	0.772 s	0.879 s	0.768 s	-12.3%	-0.262%	-12.8%

5.3.3 Other Sources of Uncertainty

Within the specimen fabrication, there were small air bubbles (on the order of 100 μm in diameter) on the specimen when being pulled as seen in Figure 16. The bubbles would sometimes appear over time during the test, even though bubbles were not visible in the original specimens prior to testing. The largest bubbles typically measure approximately 0.3 mm in diameter. Overall, the bubbles are sparse and a single clot may have as many

as 10 on the surface of the clot ranging from 0.18 mm to 0.30 mm in diameter. None of the bubbles ruptured or created tears in the clot.

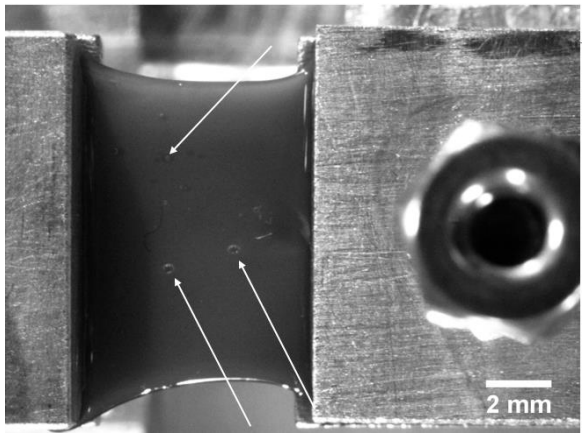

Figure 16. Top view image of bubbles present in the clot pull.

Figure 17 shows that the clot spills over the clamp when being secured in the apparatus. Small force components can be attributed to the blood surface tension with the clamp as a wetted meniscus. All of the clots behaved this way with plasma leaking out of the sides, but it is difficult to quantify the adhesion affected clot strength. The current assumption is that the plasma adhesion force is the same for all specimen tests. The test was not performed under controlled temperature or humidity, and the lack of controlled environment may have allowed the clot to dry and shrink over time.

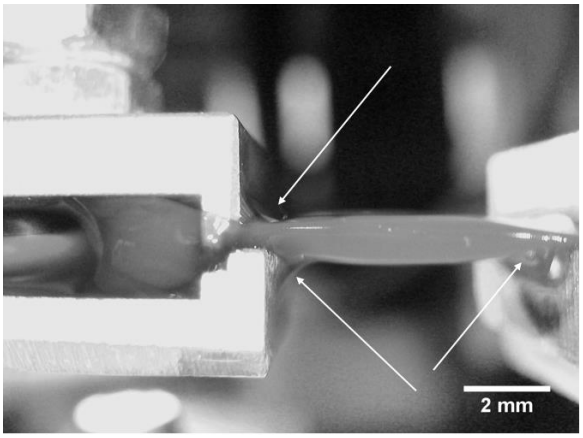

Figure 17. Side image of blood adhering to the clamp creating a wetted meniscus.

The extent and uniformity of mixing are difficult to verify, because different volumes were used to obtain the desired treatment concentration. The assumption is that all samples are evenly mixed, meaning the thrombin, calcium chloride, and inhibitors were equal throughout the clot. There is a possibility that nonuniform mixing for blebbistatin was more pronounced, because the blebbistatin clot uses a larger volume of 53 µL to mix for a final concentration of 300 µM, whereas cytochalasin uses a volume 12 µL to mix for a final concentration of 10 µM.

The 300 µM blebbistatin and 10 µM cytochalasin are assumed to inhibit all myosin II and actin respectively. Since there is only one dosage performed for each treatment, the effects are possibly dose dependent [29], [58]. There is an uncertainty if the dosages were used at a toxic level and potentially causing adverse effects on the blood clot. From similar literature, Tutwiler et al. used 200 µM blebbistatin in their studies of clot contraction [9]. Ayala et al. used 5 µM of cytochalasin D and 10 µM of blebbistatin and found that in rheometry the results were the opposite, by showing that cytochalasin affected the clot more with only 5 µM concentration [29]. However, Crow et al. used 500

nM of cytochalasin and 30 μM blebbistatin to conclude that blebbistatin affected the clot contraction more at those concentrations [35]. In this same research by Crow, 1 μM cytochalasin and 50 μM blebbistatin concentrations were found to inhibit all contraction in the clot.

6. CONCLUSIONS

6.1 Addressing the Hypothesis

The hypothesis asserted that blebbistatin affects the stiffness and viscoelastic response of blood clots more than cytochalasin D, because myosin II plays a larger role than actin in affecting the mechanical strength of the clot. The variability of nonlinear stiffness for each individual donor was substantial, for example the C_1 parameter which affects the maximum true stress, had a variation as large as 61% for whole blood. However, the nonlinear stiffness in terms of true stress vs. stretch ratio averaged across five donors showed that blebbistatin affected the clot maximum true stress at 1.5 stretch ratio by 4.3% more than cytochalasin. The 4.3% difference is greater than the calculated 1.6% uncertainty associated with quantifying true stress. From the averaged viscoelastic parameters at each increment of elongation, blebbistatin decayed more rapidly than cytochalasin, with a 10% shorter time constant at 4 mm elongation. Both the nonlinear stiffness and stress relaxation revealed similar results, which were consistent with biophysical reasoning that the myosin II inhibition prevents the cross-linking of the actin and myosin travel on actin, thus influencing structural behavior to a greater extent than cytochalasin.

Differences between the inhibitor-treated specimens were detectable with a tensile testing methodology. There was no statistically significant difference ($\alpha = 0.01$) found across five different donors. The time constant for cytochalasin was slower than the time constant for whole blood by 3.5% at 5 mm and 6.9% at 6 mm.

6.2 Recommendations for Future Work

Based on this work, a climate controlled environment is recommended to minimize possible environmental effects on the specimen during testing. A different actuator can be used, because the apparatus only needs a few millimeters of travel. Greater consistency can be achieved by using a programmable actuator that could pull and allow for 30 s of stress relaxation, instead of manually timing the pull start and stop sequence. An integrated system to activate the actuator, initiate data acquisition, take the side-view images, and the top view images could reduce possible errors introduced by operator. The clamps can be improved by developing a way to achieve constant prescribed force (magnetic or otherwise). A shorter initial working length will prevent unwanted specimen sag on clamps to start at a proper length for more consistent results. In the stress relaxation analysis, the viscoelastic model in this thesis uses force over time, which does not account for overly large clots to cause a slower stress relaxation time constant. A stress over time standard linear model may provide different results, because the area can be normalize to provide a more precise comparison between treatments [59]. The tensile testing approach with clamps allows for a more in depth understanding of clots and other soft biological materials in the micromechanical scale.

A minimum threshold is needed to understand when the drugs will interact with the clot. The established threshold will allow for a controlled change in parameters to avoid studying unwanted treatment effects not related to the desired mechanism. After minimum drug concentrations have been established, a two factor, three level factorial design of experiments can be conducted. The three levels would be low, medium, and

high doses of each treatment to check for the required threshold to inhibit all activity or extrema, and to also reveal possibly nonlinear interactions.

A different approach to supplement the testing is to use Western blotting [60] to corroborate and verify the effects of both drugs. The test can have the same four treatments of whole blood, blebbistatin, cytochalasin D, and the blebbistatin plus cytochalasin. The protein markers can be made to view the myosin II and the actin II for each treatment and compare gels for each treatment. If the gel is more pronounced then there is an indication of a higher concentration. A visual representation can be obtained by staining the platelets to highlight the actin and myosin II proteins.

REFERENCES CITED

[1] X. Liang, I. Chernysh, P. K. Purohit, and J. W. Weisel, "Phase transitions during compression and decompression of clots from platelet-poor plasma, platelet-rich plasma and whole blood," *Acta Biomater.*, vol. 60, pp. 275–290, Sep. 2017.

[2] A. E. X. Brown, R. I. Litvinov, D. E. Discher, P. K. Purohit, and J. W. Weisel, "Multiscale mechanics of fibrin polymer: gel stretching with protein unfolding and loss of water," *Science*, vol. 325, no. 5941, pp. 741–744, Aug. 2009.

[3] F. Fleissner, M. Bonn, and S. H. Parekh, "Microscale spatial heterogeneity of protein structural transitions in fibrin matrices," *Sci Adv*, vol. 2, no. 7, p. e1501778, Jul. 2016.

[4] N. Krasokha *et al.*, "Mechanical properties of blood clots – a new test method. Mechanische Eigenschaften von Thromben – Neue Untersuchungsmethoden," *Mat.-wiss. u. Werkstofftech.*, vol. 41, no. 12, pp. 1019–1024, Dec. 2010.

[5] D. R. Kumar, E. Hanlin, I. Glurich, J. J. Mazza, and S. H. Yale, "Virchow's contribution to the understanding of thrombosis and cellular biology," *Clin. Med. Res.*, vol. 8, no. 3–4, pp. 168–172, Dec. 2010.

[6] A. L. Fogelson and K. B. Neeves, "Fluid Mechanics of Blood Clot Formation," *Annu. Rev. Fluid Mech.*, vol. 47, pp. 377–403, Jan. 2015.

[7] T. H. S. van Kempen, A. C. B. Bogaerds, G. W. M. Peters, and F. N. van de Vosse, "A constitutive model for a maturing fibrin network," *Biophys. J.*, vol. 107, no. 2, pp. 504–513, Jul. 2014.

[8] P. A. Evans, K. Hawkins, and P. R. Williams, "Rheometry for blood coagulation studies," *Rheology Reviews*, vol. 2006, p. 255, 2006.

[9] V. J. Tutwiler, "Kinetics and Mechanics of Blood Clot Contraction," Doctor of Philosophy, Drexel, 2017.

[10] S. Feghhi, W. W. Tooley, and N. J. Sniadecki, "Nonmuscle Myosin IIA Regulates Platelet Contractile Forces Through Rho Kinase and Myosin Light-Chain Kinase," *J. Biomech. Eng.*, vol. 138, no. 10, Oct. 2016.

[11] R. Zhao, T. Boudou, W.-G. Wang, C. S. Chen, and D. H. Reich, "Decoupling cell and matrix mechanics in engineered microtissues using magnetically actuated microcantilevers," *Adv. Mater.*, vol. 25, no. 12, pp. 1699–1705, Mar. 2013.

[12] D. S. Gokhin, R. B. Nowak, J. A. Khoory, A. de la Piedra, I. C. Ghiran, and V. M. Fowler, "Dynamic actin filaments control the mechanical behavior of the human red blood cell membrane," *Mol. Biol. Cell*, vol. 26, no. 9, pp. 1699–1710, May 2015.

[13] A. S. Smith *et al.*, "Myosin IIA interacts with the spectrin-actin membrane skeleton to control red blood cell membrane curvature and deformability," *Proc. Natl. Acad. Sci. U. S. A.*, vol. 115, no. 19, pp. E4377–E4385, May 2018.

[14] T. Lang *et al.*, “Different effects of abciximab and cytochalasin D on clot strength in thrombelastography,” *J. Thromb. Haemost.*, vol. 2, no. 1, pp. 147–153, Jan. 2004.

[15] C. Schmitt, A. Hadj Henni, and G. Cloutier, “Characterization of blood clot viscoelasticity by dynamic ultrasound elastography and modeling of the rheological behavior,” *J. Biomech.*, vol. 44, no. 4, pp. 622–629, Feb. 2011.

[16] M. Kovács, J. Tóth, C. Hetényi, A. Málnási-Csizmadia, and J. R. Sellers, “Mechanism of Blebbistatin Inhibition of Myosin II,” *J. Biol. Chem.*, vol. 279, no. 34, pp. 35557–35563, Aug. 2004.

[17] H. Lodish, A. Berk, S. Lawrence Zipursky, P. Matsudaira, D. Baltimore, and J. Darnell, *Actin and Myosin in Nonmuscle Cells*. W. H. Freeman, 2000.

[18] A. S. Adhikari, A. H. Mekhdjian, and A. R. Dunn, “Strain tunes proteolytic degradation and diffusive transport in fibrin networks,” *Biomacromolecules*, vol. 13, no. 2, pp. 499–506, Feb. 2012.

[19] K. A. Jansen, R. G. Bacabac, I. K. Piechocka, and G. H. Koenderink, “Cells actively stiffen fibrin networks by generating contractile stress,” *Biophys. J.*, vol. 105, no. 10, pp. 2240–2251, Nov. 2013.

[20] D. M. Albala and J. H. Lawson, “Recent clinical and investigational applications of fibrin sealant in selected surgical specialties,” *J. Am. Coll. Surg.*, vol. 202, no. 4, pp. 685–697, Apr. 2006.

[21] J. W. Weisel, “The mechanical properties of fibrin for basic scientists and clinicians,” *Biophys. Chem.*, vol. 112, no. 2–3, pp. 267–276, Dec. 2004.

[22] Q. Wen, A. Basu, P. A. Janmey, and A. G. Yodh, “Non-affine deformations in polymer hydrogels,” *Soft Matter*, vol. 8, no. 31, pp. 8039–8049, Jan. 2012.

[23] J. Maitra and V. K. Shukla, “Cross-linking in Hydrogels - A Review,” *American Journal of Polymer Science*, vol. 4, no. 2, pp. 25–31, 2014.

[24] H. Babavalian, A. M. Latifi, M. A. Shokrgozar, S. Bonakdar, F. Shakeri, and H. Tebyanian, “Healing Effects of Synthetic and Commercial Alginate Hydrogel Dressings on Wounds: A Comparative Study,” *Trauma Mon*, vol. In Press, no. In Press, Aug. 2016.

[25] K. Y. Lee and D. J. Mooney, “Alginate: properties and biomedical applications,” *Prog. Polym. Sci.*, vol. 37, no. 1, pp. 106–126, Jan. 2012.

[26] J. L. Drury, R. G. Dennis, and D. J. Mooney, “The tensile properties of alginate hydrogels,” *Biomaterials*, vol. 25, no. 16, pp. 3187–3199, Jul. 2004.

[27] O. V. Kim, R. I. Litvinov, J. Chen, D. Z. Chen, J. W. Weisel, and M. S. Alber, “Compression-induced structural and mechanical changes of fibrin-collagen composites,” *Matrix Biol.*, vol. 60–61, pp. 141–156, Jul. 2017.

[28] J. L. Velada, D. A. Hollingsbee, A. R. Menzies, R. Cornwell, and R. A. Dodd, "Reproducibility of the mechanical properties of Vivostat system patient-derived fibrin sealant," *Biomaterials*, vol. 23, no. 10, pp. 2249–2254, May 2002.

[29] Y. A. Ayala *et al.*, "Effects of cytoskeletal drugs on actin cortex elasticity," *Exp. Cell Res.*, vol. 351, no. 2, pp. 173–181, Feb. 2017.

[30] V. Tutwiler, H. Wang, R. I. Litvinov, J. W. Weisel, and V. B. Shenoy, "Interplay of Platelet Contractility and Elasticity of Fibrin/Erythrocytes in Blood Clot Retraction," *Biophys. J.*, vol. 112, no. 4, pp. 714–723, Feb. 2017.

[31] C. D. Markert *et al.*, "Characterizing the micro-scale elastic modulus of hydrogels for use in regenerative medicine," *J. Mech. Behav. Biomed. Mater.*, vol. 27, pp. 115–127, Nov. 2013.

[32] T. Feller, M. S. Z. Kellermayer, and B. Kiss, "Nano-thrombelastography of fibrin during blood plasma clotting," *J. Struct. Biol.*, vol. 186, no. 3, pp. 462–471, Jun. 2014.

[33] S. Baker *et al.*, "The Mechanical Properties of Dry, Electrospun Fibrinogen Fibers," *Mater. Sci. Eng. C Mater. Biol. Appl.*, vol. 32, no. 2, pp. 215–221, Mar. 2012.

[34] W. A. Lam *et al.*, "Mechanics and contraction dynamics of single platelets and implications for clot stiffening," *Nat. Mater.*, vol. 10, no. 1, pp. 61–66, Jan. 2011.

[35] A. Crow, K. D. Webster, E. Hohlfeld, W. P. Ng, P. Geissler, and D. A. Fletcher, "Contractile equilibration of single cells to step changes in extracellular stiffness," *Biophys. J.*, vol. 102, no. 3, pp. 443–451, Feb. 2012.

[36] K. C. Murphy and J. K. Leach, "A reproducible, high throughput method for fabricating fibrin gels," *BMC Res. Notes*, vol. 5, p. 423, Aug. 2012.

[37] Z. Li, X. Li, B. McCracken, Y. Shao, K. Ward, and J. Fu, "A Miniaturized Hemoretractometer for Blood Clot Retraction Testing," *Small*, vol. 12, no. 29, pp. 3926–3934, Aug. 2016.

[38] M. S. Zamil, H. Yi, M. A. Haque, and V. M. Puri, "Characterizing microscale biological samples under tensile loading: stress-strain behavior of cell wall fragment of onion outer epidermis," *Am. J. Bot.*, vol. 100, no. 6, pp. 1105–1115, Jun. 2013.

[39] K. Kim, H. Yi, M. S. Zamil, M. A. Haque, and V. M. Puri, "Multiscale stress–strain characterization of onion outer epidermal tissue in wet and dry states," *Am. J. Bot.*, vol. 102, no. 1, pp. 12–20, Jan. 2015.

[40] E. Jacquet, S. Joly, J. Chambert, K. Rekik, and P. Sandoz, "Ultra-light extensometer for the assessment of the mechanical properties of the human skin in vivo," *Skin Res. Technol.*, vol. 23, no. 4, pp. 531–538, Nov. 2017.

[41] R. Krone, K. Havenstrite, and B. Shafi, "Mechanical characterization of thin film, water-based polymer gels through simple tension testing of laminated bilayers," *J. Mech. Behav. Biomed. Mater.*, vol. 27, pp. 1–9, Nov. 2013.

[42] W. C. Nelson and C.-J. “cj” Kim, “Droplet Actuation by Electrowetting-on-Dielectric (EWOD): A Review,” *J. Adhes. Sci. Technol.*, vol. 26, no. 12–17, pp. 1747–1771, Sep. 2012.

[43] K. Choi, A. H. C. Ng, R. Fobel, and A. R. Wheeler, “Digital microfluidics,” *Annu. Rev. Anal. Chem.* , vol. 5, pp. 413–440, Jan. 2012.

[44] S. M. George and H. Moon, “Digital microfluidic three-dimensional cell culture and chemical screening platform using alginate hydrogels,” *Biomicrofluidics*, vol. 9, no. 2, p. 024116, Mar. 2015.

[45] A. R. Wufsus, N. E. Macera, and K. B. Neeves, “The hydraulic permeability of blood clots as a function of fibrin and platelet density,” *Biophys. J.*, vol. 104, no. 8, pp. 1812–1823, Apr. 2013.

[46] A. Srinivasan, K. P. Leung, J. L. Lopez-Ribot, and A. K. Ramasubramanian, “High-throughput nano-biofilm microarray for antifungal drug discovery,” *MBio*, vol. 4, no. 4, Jun. 2013.

[47] A. Srinivasan, P. Uppuluri, J. Lopez-Ribot, and A. K. Ramasubramanian, “Development of a high-throughput Candida albicans biofilm chip,” *PLoS One*, vol. 6, no. 4, p. e19036, Apr. 2011.

[48] Y. C. Fung, “Structure and Stress-Strain Relationship of Soft Tissues1,” *Am. Zool.*, vol. 24, pp. 13–22, 1984.

[49] M. A. Kotlarchyk *et al.*, “Concentration independent modulation of local micromechanics in a fibrin gel,” *PLoS One*, vol. 6, no. 5, p. e20201, May 2011.

[50] K. J. Haworth, C. R. Weidner, T. A. Abruzzo, J. T. Shearn, and C. K. Holland, “Mechanical properties and fibrin characteristics of endovascular coil-clot complexes: relevance to endovascular cerebral aneurysm repair paradigms,” *J. Neurointerv. Surg.*, vol. 7, no. 4, pp. 291–296, Apr. 2015.

[51] A. N. Natali, E. L. Carniel, P. G. Pavan, P. Dario, and I. Izzo, “Hyperelastic models for the analysis of soft tissue mechanics: definition of constitutive parameters,” in *The First IEEE/RAS-EMBS International Conference on Biomedical Robotics and Biomechatronics, 2006. BioRob 2006.*, Pisa, Italy, pp. 188–191.

[52] R. Keerthiwansa, J. Javorik, J. Kledrowetz, and P. Nekoksa, “Elastomer testing: the risk of using only uniaxial data for fitting the Mooney-Rivlin hyperelastic-material model,” *Mater. Tehnol.*, vol. 52, no. 1, pp. 3–8, Feb. 2018.

[53] J. C. Iatridis, J. Wu, J. A. Yandow, and H. M. Langevin, “Subcutaneous tissue mechanical behavior is linear and viscoelastic under uniaxial tension,” *Connect. Tissue Res.*, vol. 44, no. 5, pp. 208–217, 2003.

[54] C. Ross Ethier and C. A. Simmons, *Introductory Biomechanics: From Cells to Organisms*. Cambridge University Press, 2007.

[55] T. H. S. van Kempen, W. P. Donders, F. N. van de Vosse, and G. W. M. Peters, “A constitutive model for developing blood clots with various compositions and their nonlinear viscoelastic behavior,” *Biomech. Model. Mechanobiol.*, vol. 15, no. 2, pp. 279–291, Apr. 2016.

[56] S. de Gelidi, G. Tozzi, and A. Bucchi, “The effect of thickness measurement on numerical arterial models,” *Mater. Sci. Eng. C Mater. Biol. Appl.*, vol. 76, pp. 1205–1215, Jul. 2017.

[57] J. Schindelin *et al.*, “Fiji: an open-source platform for biological-image analysis,” *Nat. Methods*, vol. 9, no. 7, pp. 676–682, Jun. 2012.

[58] Y. Hayashi, M.-A. Brun, K. Machida, and M. Nagasawa, “Principles of dielectric blood coagulometry as a comprehensive coagulation test,” *Anal. Chem.*, vol. 87, no. 19, pp. 10072–10079, Oct. 2015.

[59] Y. M. Efremov, W.-H. Wang, S. D. Hardy, R. L. Geahlen, and A. Raman, “Measuring nanoscale viscoelastic parameters of cells directly from AFM force-displacement curves,” *Sci. Rep.*, vol. 7, no. 1, p. 1541, May 2017.

[60] S.-I. Arimura *et al.*, “Hydroxyapatite formed on/in agarose gel induces activation of blood coagulation and platelets aggregation,” *J. Biomed. Mater. Res. B Appl. Biomater.*, vol. 81, no. 2, pp. 456–461, May 2007.

APPENDIX A: APPARATUS TECHNICAL DOCUMENTS

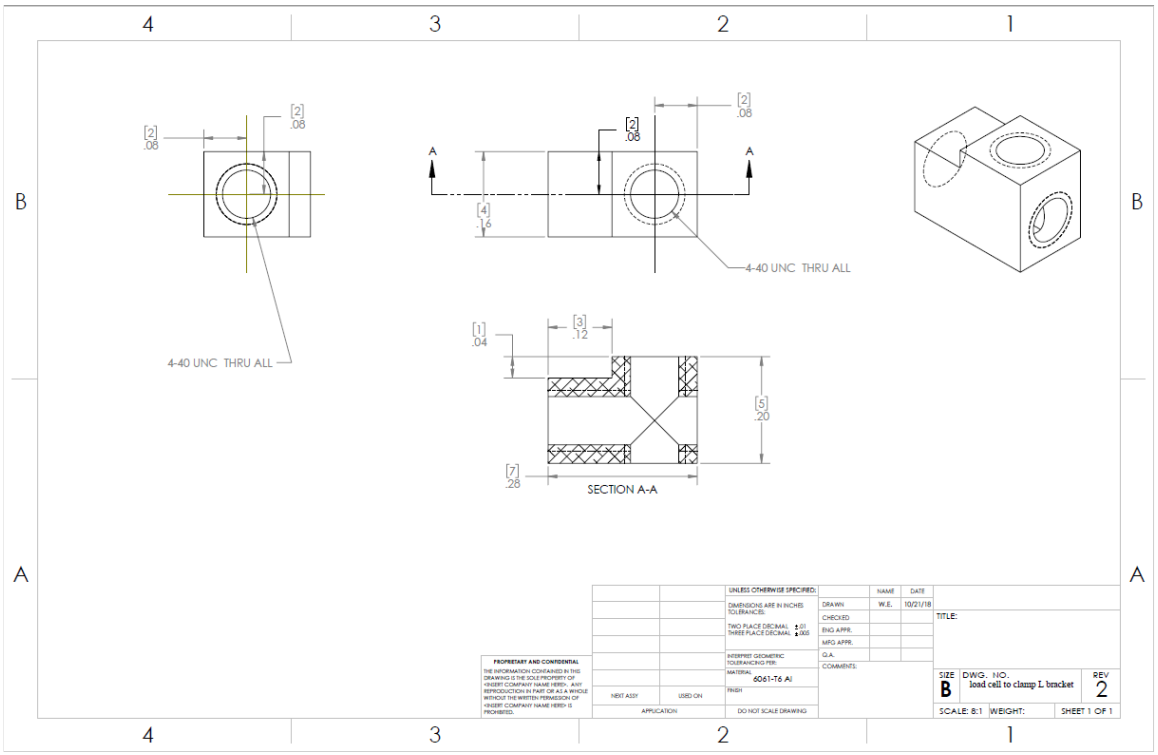

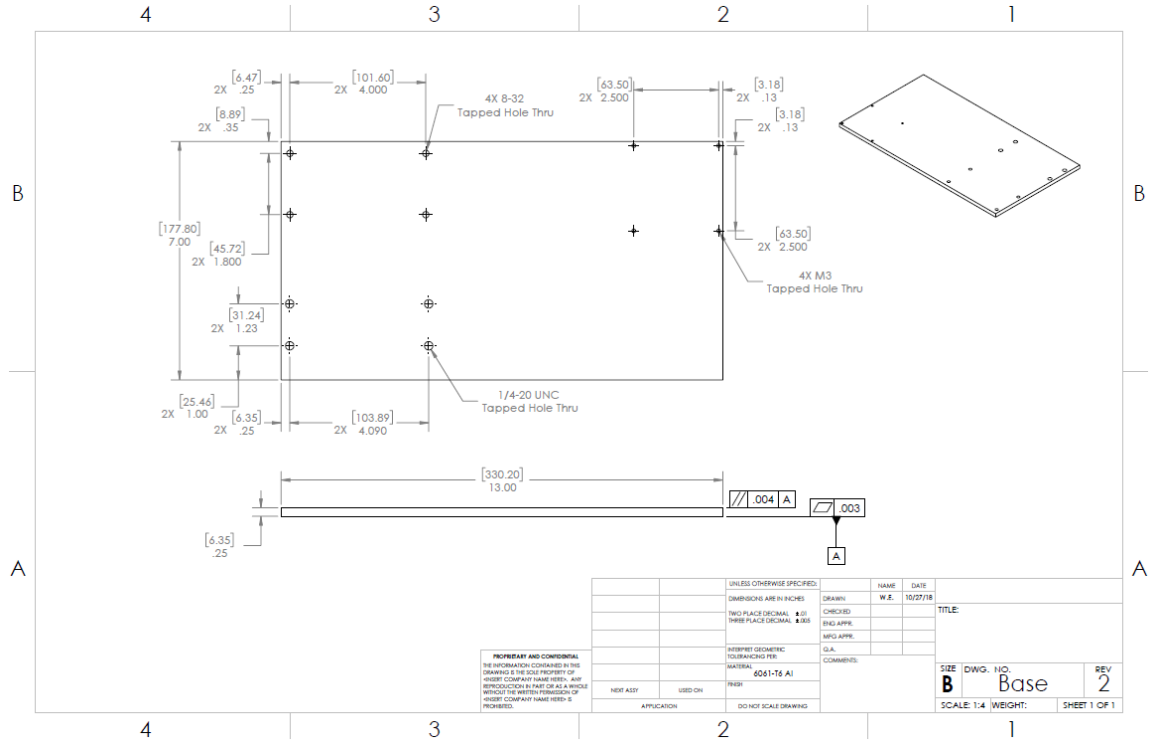

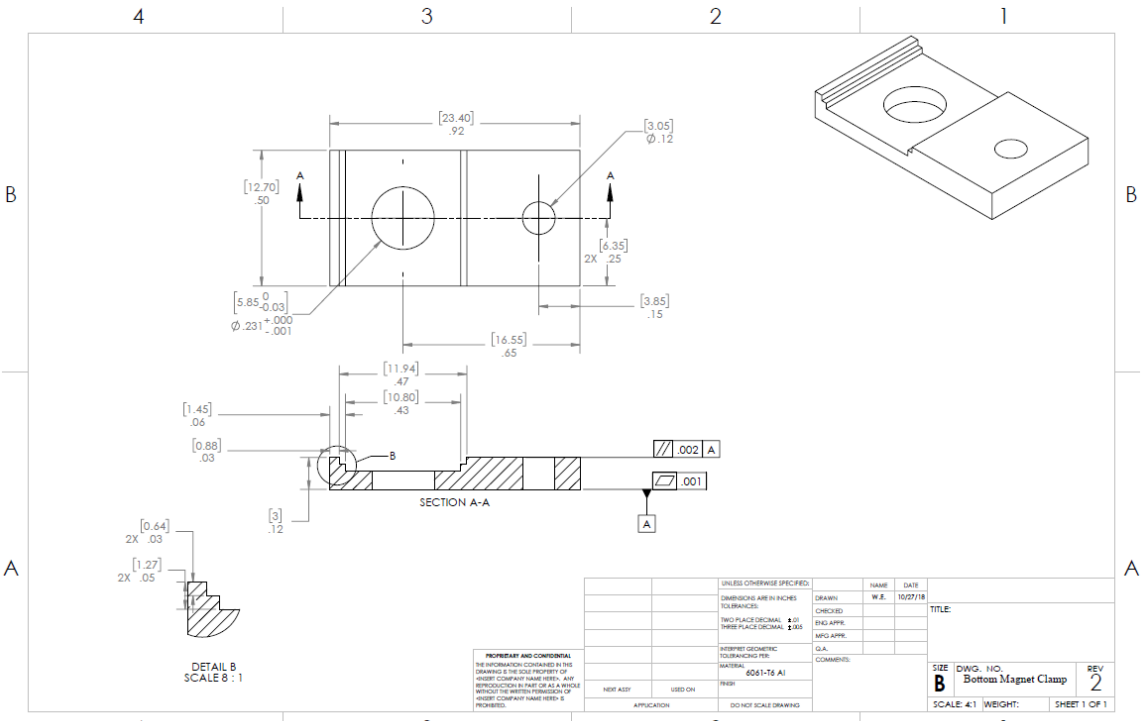
4
3
2
1
B
A
[23.40] .92
[3.05] Ø.12
[12.70] .50
A
A
[6.35] 2X .25
[5.85 0 -0.03] Ø.231 .000 -.001
[3.85] .15
[16.55] .65
[11.94] .47
[10.80] .43
[1.45] .06
[0.88] .03
B
.002 A
.001
A
SECTION A-A
[3] .12
[0.64] 2X .03
[1.27] 2X .05
DETAIL B
SCALE 8 : 1
UNLESS OTHERWISE SPECIFIED:
DIMENSIONS ARE IN INCHES
TOLERANCES:
TWO PLACE DECIMAL ±.01
THREE PLACE DECIMAL ±.005
INTERPRET GEOMETRIC TOLERANCING PER:
MATERIAL
6061-T6 Al
FINISH
NEXT ASSY
USED ON
APPLICATION
DO NOT SCALE DRAWING
NAME
DATE
DRAWN
W.E.
10/27/18
CHECKED
ENG APPR.
MFG APPR.
Q.A.
COMMENTS:
TITLE:
SIZE
B
DWG. NO.
Bottom Magnet Clamp
REV
2
SCALE: 4:1
WEIGHT:
SHEET 1 OF 1
PROPRIETARY AND CONFIDENTIAL
THE INFORMATION CONTAINED IN THIS DRAWING IS THE SOLE PROPERTY OF <INSERT COMPANY NAME HERE>. ANY REPRODUCTION IN PART OR AS A WHOLE WITHOUT THE WRITTEN PERMISSION OF <INSERT COMPANY NAME HERE> IS PROHIBITED.

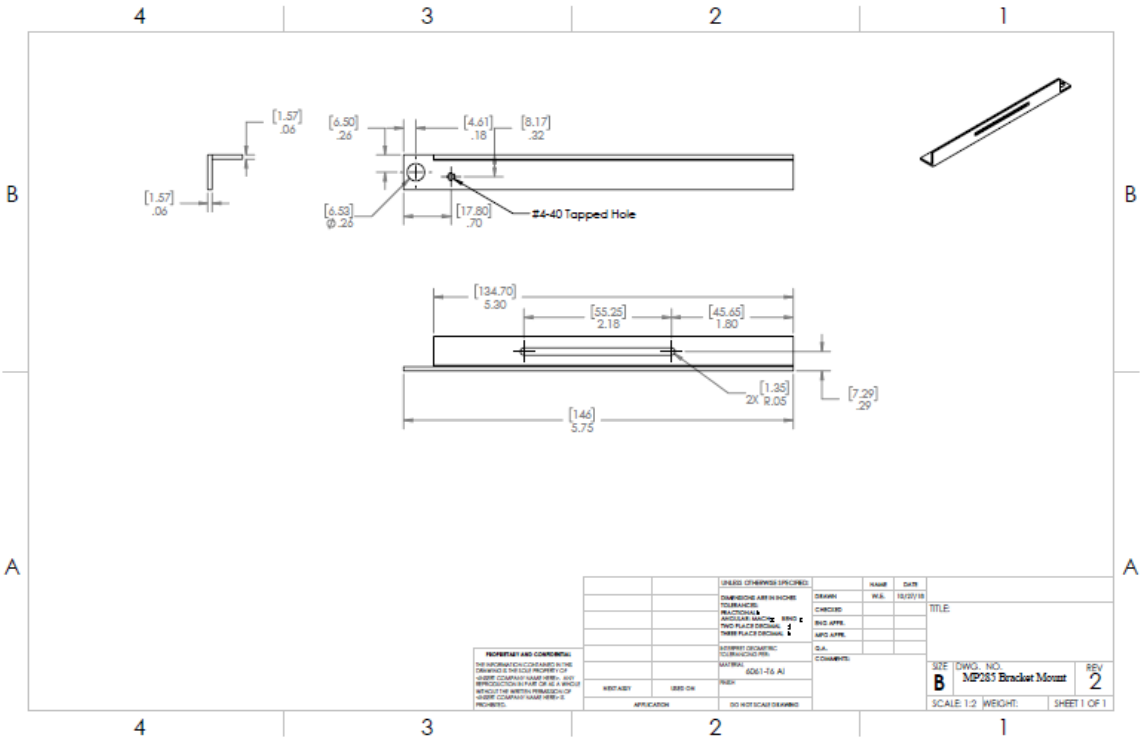
4
3
2
1
B
A
[1.57] .06
[1.57] .06
[6.50] .26
[4.61] .18
[8.17] .32
[6.53] Ø.26
[17.80] .70
#4-40 Tapped Hole
[134.70] 5.30
[55.25] 2.18
[45.65] 1.80
[1.35] 2X R.05
[7.29] .29
[146] 5.75
UNLESS OTHERWISE SPECIFIED:
DIMENSIONS ARE IN INCHES
TOLERANCES:
TWO PLACE DECIMAL ±
THREE PLACE DECIMAL ±
INTERPRET GEOMETRIC TOLERANCING PER:
MATERIAL
6061-T6 Al
FINISH
NEXT ASSY
USED ON
APPLICATION
DO NOT SCALE DRAWING
NAME
DATE
DRAWN
W.E.
10/27/18
CHECKED
ENG APPR.
MFG APPR.
Q.A.
COMMENTS:
TITLE:
SIZE
B
DWG. NO.
MP283 Bracket Mount
REV
2
SCALE: 1:2
WEIGHT:
SHEET 1 OF 1
PROPRIETARY AND CONFIDENTIAL

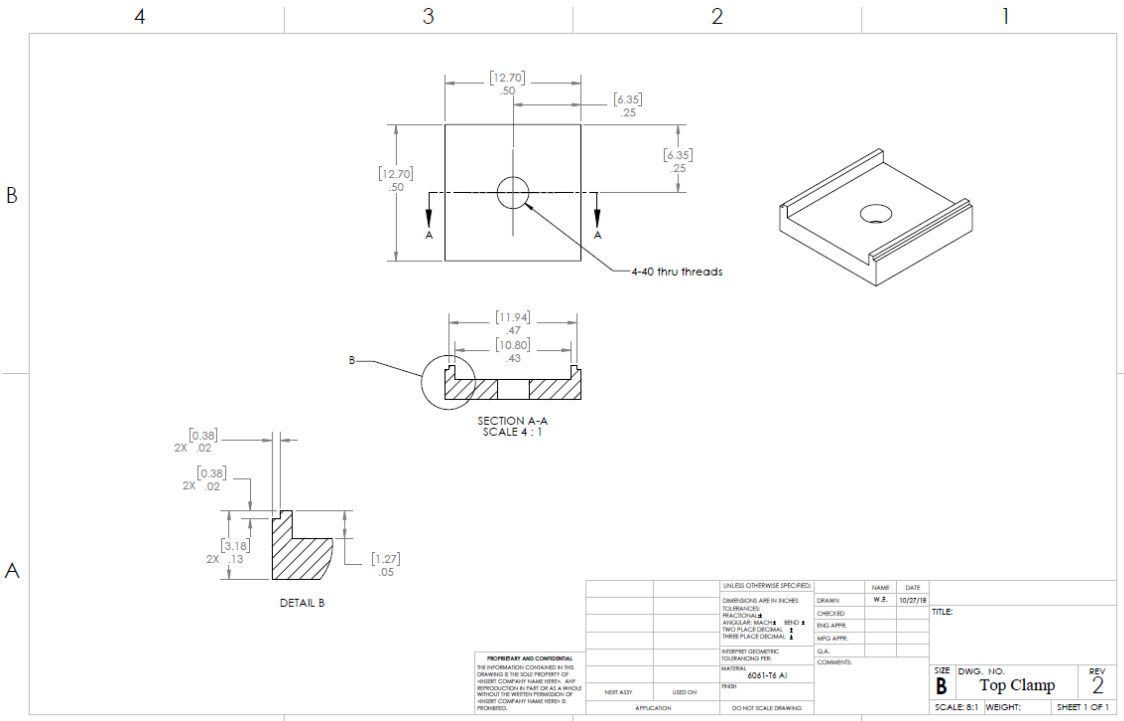
4
3
2
1
B
A
[12.70]
.50
[6.35]
.25
[6.35]
.25
[12.70]
.50
A
A
4-40 thru threads
[11.94]
.47
[10.80]
.43
B
SECTION A-A
SCALE 4 : 1
[0.38]
2X .02
[0.38]
2X .02
[3.18]
2X .13
[1.27]
.05
DETAIL B
UNLESS OTHERWISE SPECIFIED:
DIMENSIONS ARE IN INCHES
TOLERANCES:
FRACTIONAL
ANGULAR: MACH BEND
TWO PLACE DECIMAL
THREE PLACE DECIMAL
INTERPRET GEOMETRIC TOLERANCING PER:
MATERIAL
6061-T6 Al
FINISH
NEXT ASSY
USED ON
APPLICATION
DO NOT SCALE DRAWING
NAME
DATE
DRAWN
W.E.
10/27/18
CHECKED
ENG APPR.
MFG APPR.
Q.A.
COMMENTS:
TITLE:
PROPRIETARY AND CONFIDENTIAL
THE INFORMATION CONTAINED IN THIS DRAWING IS THE SOLE PROPERTY OF <INSERT COMPANY NAME HERE>. ANY REPRODUCTION IN PART OR AS A WHOLE WITHOUT THE WRITTEN PERMISSION OF <INSERT COMPANY NAME HERE> IS PROHIBITED.
SIZE
B
DWG. NO.
Top Clamp
REV
2
SCALE: 8:1
WEIGHT:
SHEET 1 OF 1

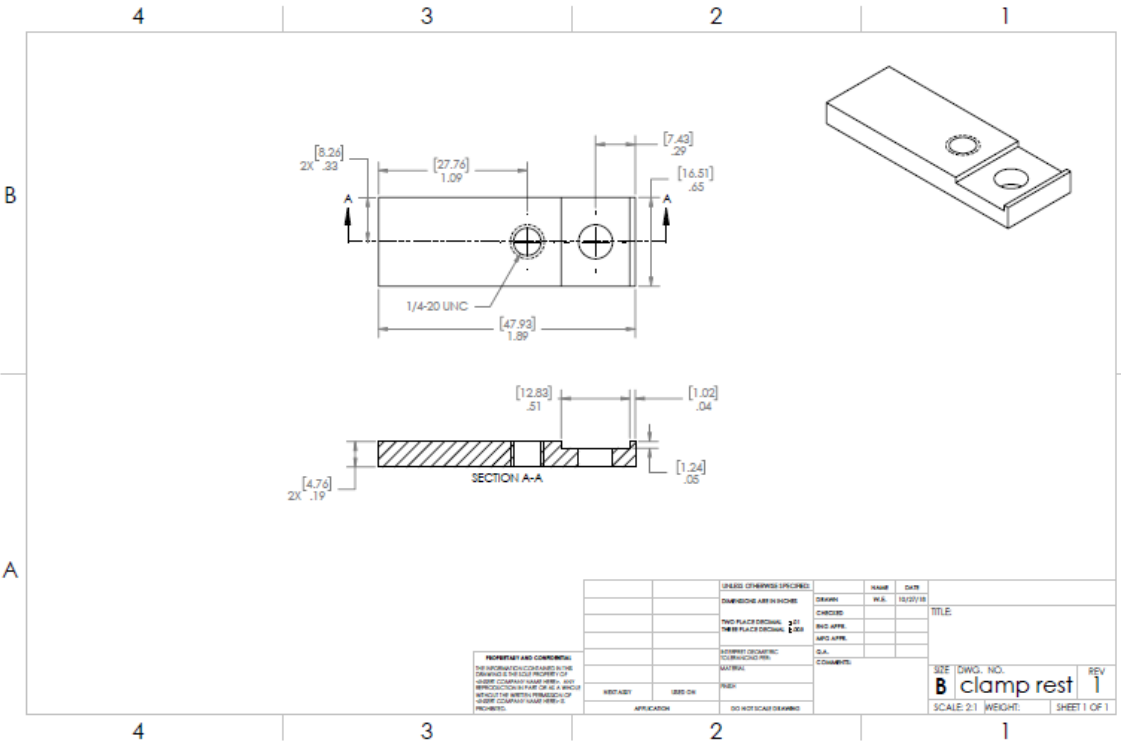
4
3
2
1
B
A
[8.26]
2X .33
[27.76]
1.09
[7.43]
.29
[16.51]
.65
A
A
1/4-20 UNC
[47.93]
1.89
[12.83]
.51
[1.02]
.04
[1.24]
.05
[4.76]
2X .19
SECTION A-A
UNLESS OTHERWISE SPECIFIED:
DIMENSIONS ARE IN INCHES
TWO PLACE DECIMAL
THREE PLACE DECIMAL
INTERPRET GEOMETRIC TOLERANCING PER:
MATERIAL
FINISH
NEXT ASSY
USED ON
APPLICATION
DO NOT SCALE DRAWING
NAME
DATE
DRAWN
W.A.
10/27/18
CHECKED
ENG APPR.
MFG APPR.
Q.A.
COMMENTS:
TITLE:
PROPRIETARY AND CONFIDENTIAL
SIZE
B
DWG. NO.
clamp rest
REV
1
SCALE: 2:1
WEIGHT:
SHEET 1 OF 1

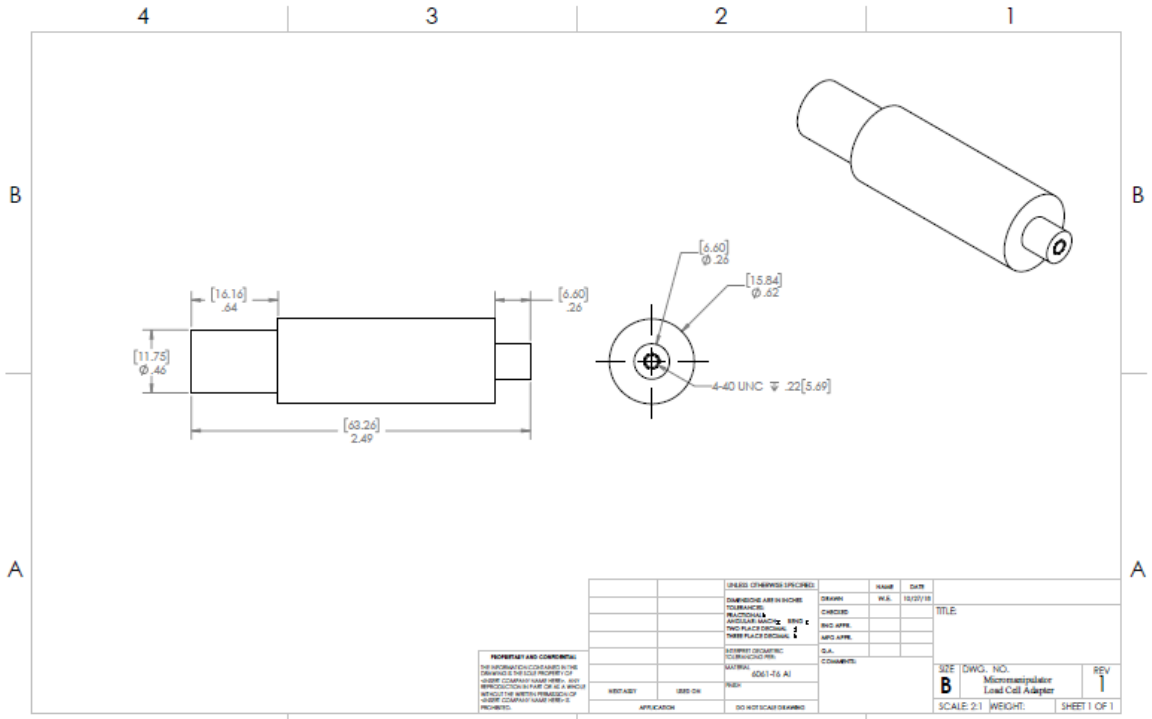
[16.16]
.64
[6.60]
.26
[11.75]
Ø .46
[63.26]
2.49
[6.60]
Ø .26
[15.84]
Ø .62
4-40 UNC ↧ .22[5.69]
UNLESS OTHERWISE SPECIFIED:
DIMENSIONS ARE IN INCHES
TOLERANCES:
FRACTIONAL
ANGULAR: MACH ± BEND ±
TWO PLACE DECIMAL ±
THREE PLACE DECIMAL ±
INTERPRET GEOMETRIC TOLERANCING PER:
MATERIAL
6061-T6 Al
FINISH
NEXT ASSY
USED ON
APPLICATION
DO NOT SCALE DRAWING
NAME
DATE
DRAWN
W.E.
10/27/18
CHECKED
ENG APPR.
MFG APPR.
Q.A.
COMMENTS:
TITLE:
PROPRIETARY AND CONFIDENTIAL
THE INFORMATION CONTAINED IN THIS DRAWING IS THE SOLE PROPERTY OF <INSERT COMPANY NAME HERE>. ANY REPRODUCTION IN PART OR AS A WHOLE WITHOUT THE WRITTEN PERMISSION OF <INSERT COMPANY NAME HERE> IS PROHIBITED.
SIZE
B
DWG. NO.
Micromanipulator
Load Cell Adapter
REV
1
SCALE: 2:1
WEIGHT:
SHEET 1 OF 1

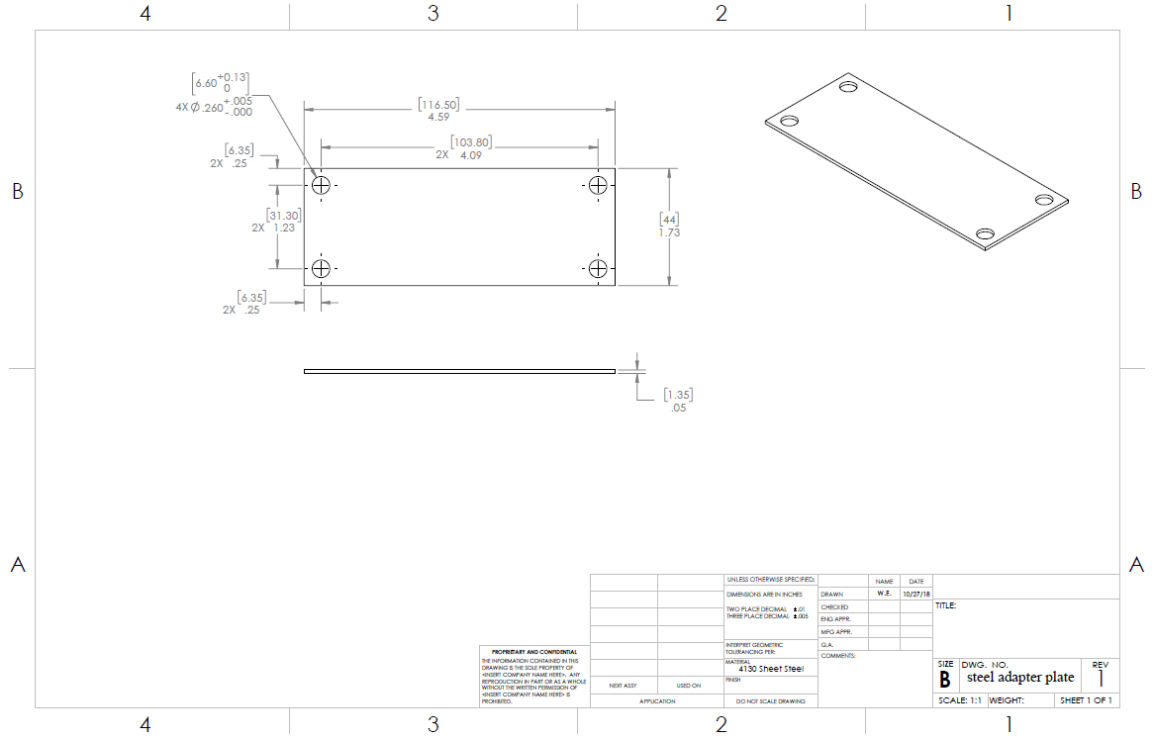
[6.60 +0.13 0]
4X Ø .260 +.005 -.000
[116.50]
4.59
[103.80]
2X 4.09
[6.35]
2X .25
[31.30]
2X 1.23
[44]
1.73
[6.35]
2X .25
[1.35]
.05
UNLESS OTHERWISE SPECIFIED:
DIMENSIONS ARE IN INCHES
TWO PLACE DECIMAL ±.01
THREE PLACE DECIMAL ±.005
INTERPRET GEOMETRIC TOLERANCING PER:
MATERIAL
4130 Sheet Steel
FINISH
NEXT ASSY
USED ON
APPLICATION
DO NOT SCALE DRAWING
NAME
DATE
DRAWN
W.E.
10/27/18
CHECKED
ENG APPR.
MFG APPR.
Q.A.
COMMENTS:
TITLE:
PROPRIETARY AND CONFIDENTIAL
THE INFORMATION CONTAINED IN THIS DRAWING IS THE SOLE PROPERTY OF <INSERT COMPANY NAME HERE>. ANY REPRODUCTION IN PART OR AS A WHOLE WITHOUT THE WRITTEN PERMISSION OF <INSERT COMPANY NAME HERE> IS PROHIBITED.
SIZE
B
DWG. NO.
steel adapter plate
REV
1
SCALE: 1:1
WEIGHT:
SHEET 1 OF 1

APPENDIX B: GLOSSARY

Alginate - An extract from brown seaweed cell walls that can be mixed with calcium and sodium salts to create a flexible fibre.

Actin - A thin protein in the cytoskeleton that interacts with myosin II in a primitive sarcomere like.

Aneurysm - A localized region in a blood vessel that is abnormally large due to thrombosis or embolization which is a piece of material inside the blood vessel causing blockage.

Blebbistatin - A myosin inhibitor for myosin II which would prevent ATP, resulting in a low energy state.

Coagulation - The process of blood changing from a liquid to a solid with the activation of platelets and fibrin to form a clot. Thrombosis or hemorrhaging can occur due to coagulation clotting issues.

Collagen - A main structural protein that can be found throughout the body.

Clot - Solidified blood.

Cytochalasin - A fungal mobilite that can block and inhibit polymerization and elongation of actin.

Cytochalasin D - Inhibits actin polymerization by capping the ends of the actin chain.

Denaturation - A process where proteins can lose structure, typically caused by the environment such as heat or a chemical reaction.

Eptifibatide - An antiplatelet drug that prevents blood from clotting and be used for heart attacks in people with severe chest pains.

Factor XIII (FXIII) - Also known as fibrin stabilizing factor, is an enzyme that will cross-link fibrin.

Fibrin - A fibrous protein formed from thrombin and fibrinogen. The protein can be polymerized with platelets to form a clot over a wound.

Fibrinogen - Also known as factor I and when combined with thrombin it forms a fibrin based blood clot.

Fibrinolysis - Prevents blood clots from growing too large and becoming problematic. The fibrin clot is broken down and the remains are cleared by proteases or by organs like the kidney or liver.

Fibroblasts - Synthesizes extracellular matrix and collagen, which is critical to wound healing.

FFP (Fresh Frozen Plasma) - Liquid portion of whole blood that can be used to treat conditions with low blood clotting factors.

Hemarthrosis - Bleeding in the joints due to lack of factor XIII.

Hemophilia - The ability to have blood clot is severely reduced relative to normal population due to missing clotting factors.

Hemostatic- An antihemorrhagic agent that contracts tissue to seal wounds.

Hydrogel - A gel with water as the main liquid, can be used in biological functions to help with wound healing.

Ischemic - Restricted blood flow to regions causing a lack of oxygen needed for basic cellular metabolism.

Lysis - Breaking down.

Myocardial infarction - Another term for heart attack which happens when there is restricted blood flow to the heart, causing damage to the heart.

Myosin II - A protein that assists in providing cellular structure by binding and traveling along actin filaments.

Plasma - Contributes to 55% of the body's total blood volume which contains dissolved proteins such as fibrinogen. Also contains proteins, ions, nutrients, and waste.

Platelet - Also known as thrombocytes and is a component of blood that can clump and clot blood.

PRP (Platelet Rich Plasma) - A concentration from whole blood. Platelet-rich plasma is centrifuged to remove red blood cells. Has a greater concentration of cellular growth factors (e.g. PDGF, IGF-1, EGF, and TGF-beta) activating fibroblasts.

PPP (Platelet Poor Plasma) - Blood plasma with a low number of platelets that can have an elevated level of fibrinogen.

Stroke - Restricted blood flow due to ischemia or hemorrhage where there is bleeding in the skull.

Thrombin - Acts as a serine protease that converts soluble fibrinogen into insoluble strands of fibrin.

Thrombosis - Formation of a blood clot in a blood vessel with platelets and fibrin.

Thrombolysis - Breakdown of a blood clot in a blood vessel.

APPENDIX C: EXPERIMENTAL PLOTS

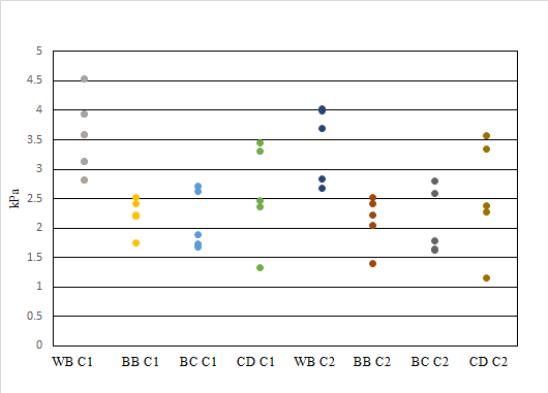

Mooney-Rivlin $C_1$and C_2parameters in dot plot form

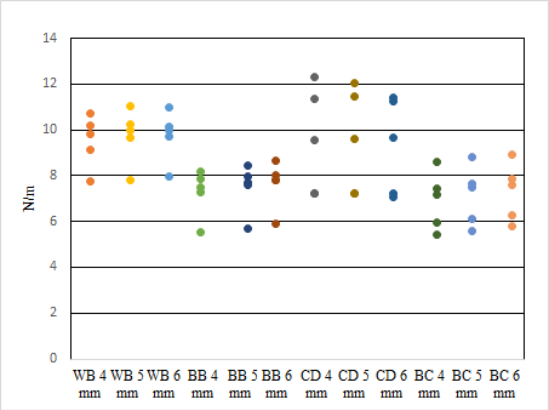

Extracted viscoelastic k_2 spring parameter at 3 second

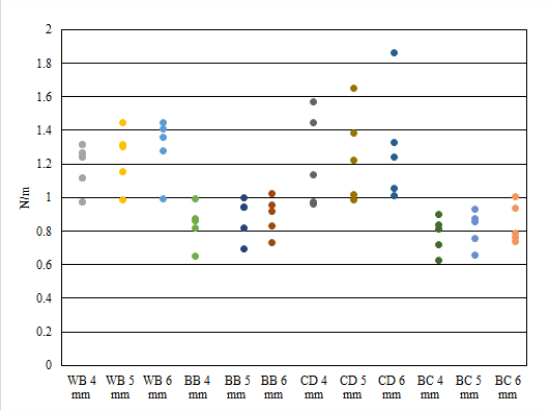

Extracted viscoelastic k_1 spring parameter at 3 s

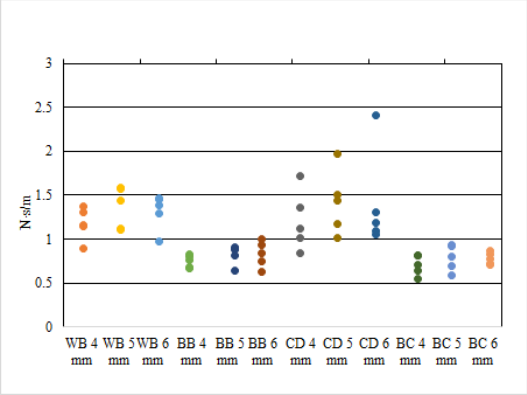

Extracted viscoelastic η spring parameter at 3 s

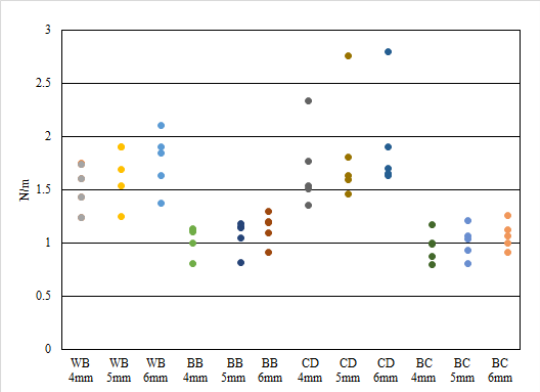

Extracted viscoelastic k_1 spring parameter at 30 s

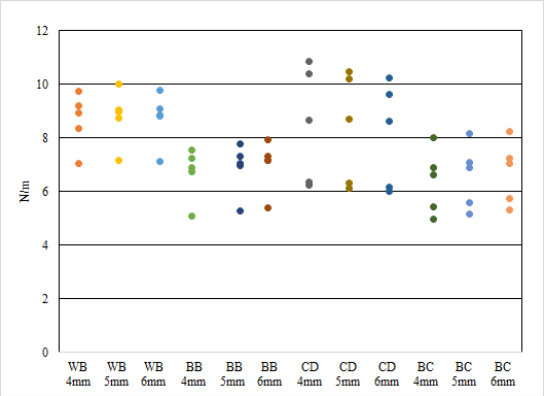

Extracted viscoelastic k_2 spring parameter at 30 s

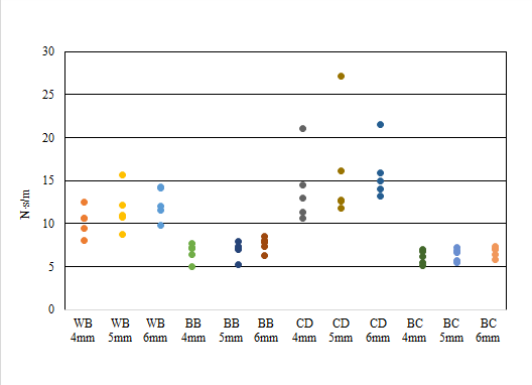

Extracted viscoelastic η spring parameter at 30 s

APPENDIX D: RAW EXPERIMENTAL IMAGES

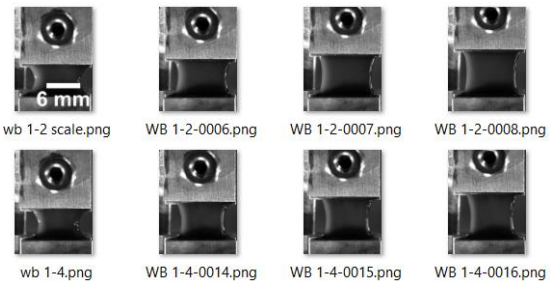

Donor 1 whole blood top view images

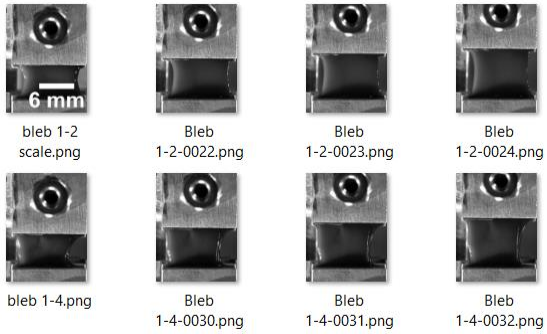

Donor 1 blebbistatin top-view images

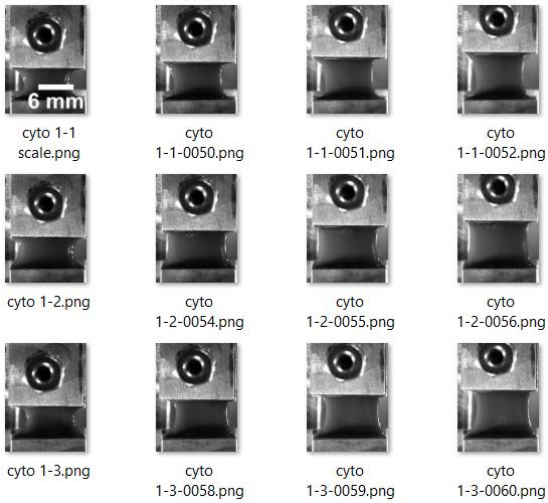

Donor 1 cytochalasin top-view images

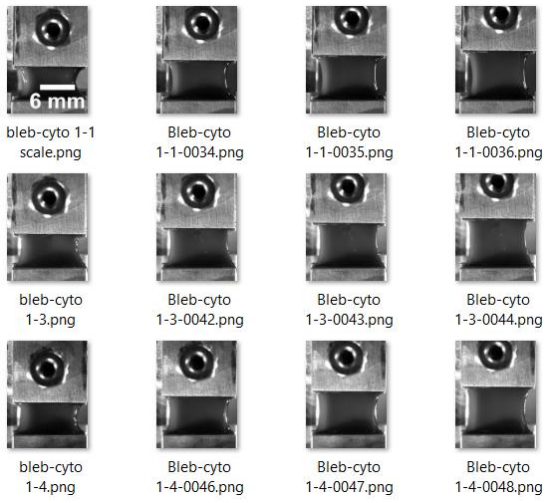

Donor 1 blebbistatin plus cytochalasin mixture top-view images

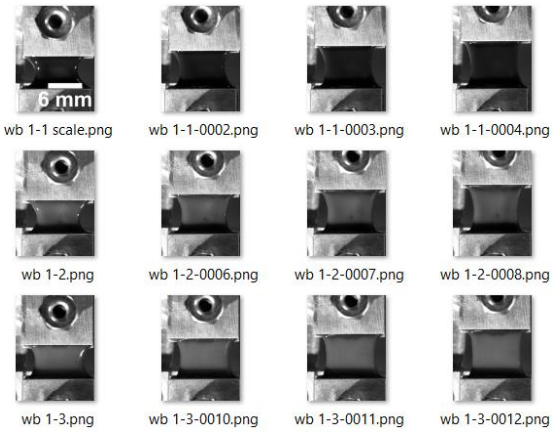

Donor 2 whole blood top-view images

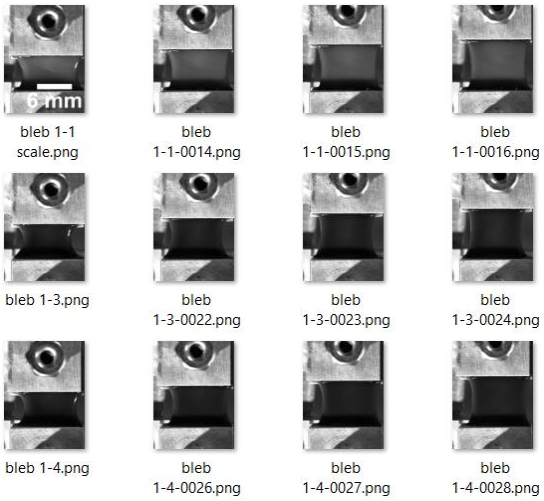

Donor 2 blebbistatin top-view images

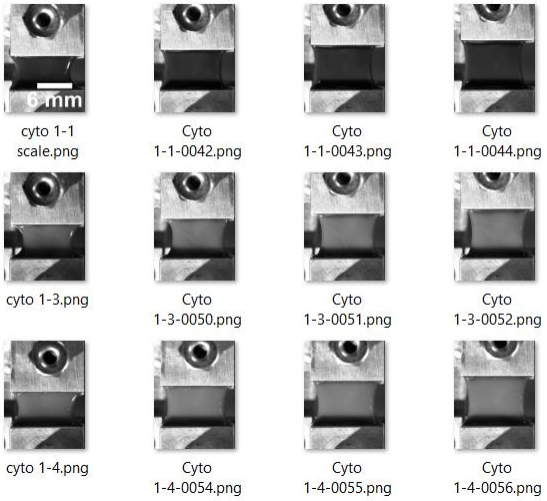

Donor 2 cytochalasin top-view images

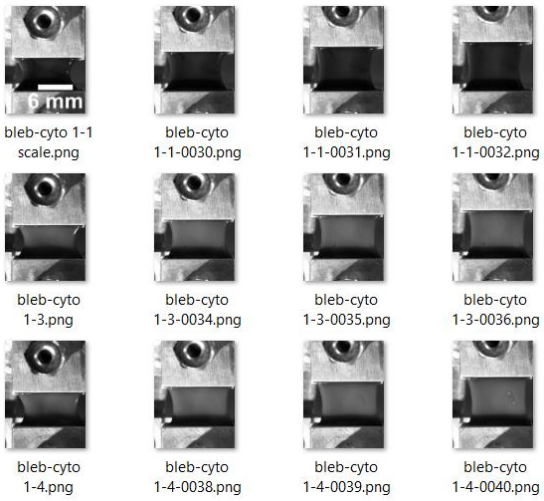

Donor 2 blebbistatin plus cytochalasin mixture top-view images

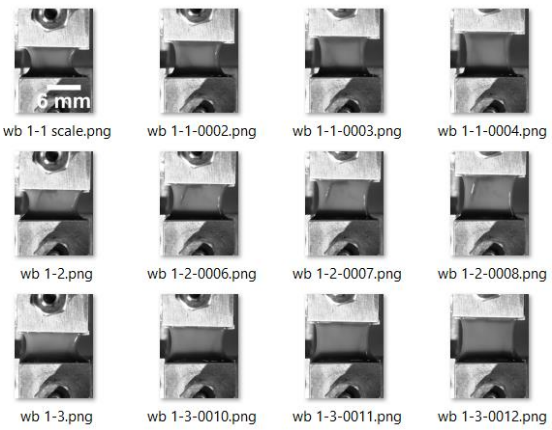

Donor 3 whole blood top-view images

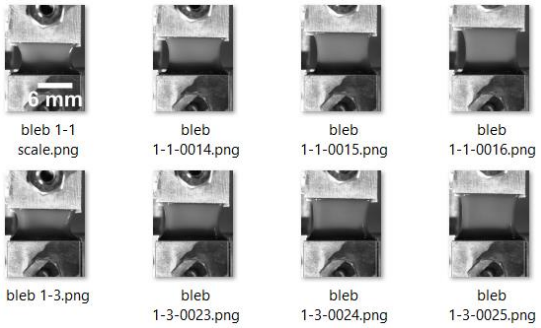

Donor 3 blebbistatin top-view images

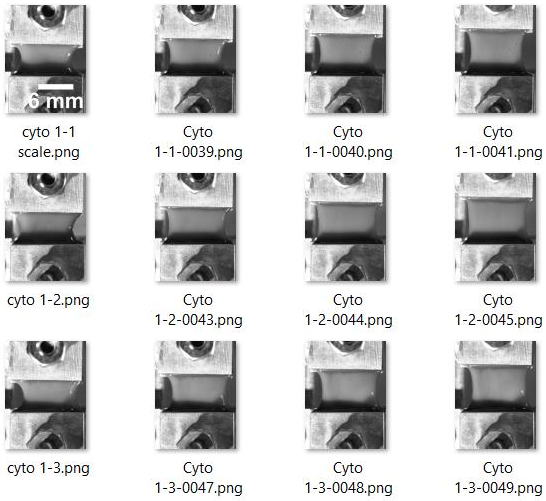

Donor 3 cytochalasin top-view images

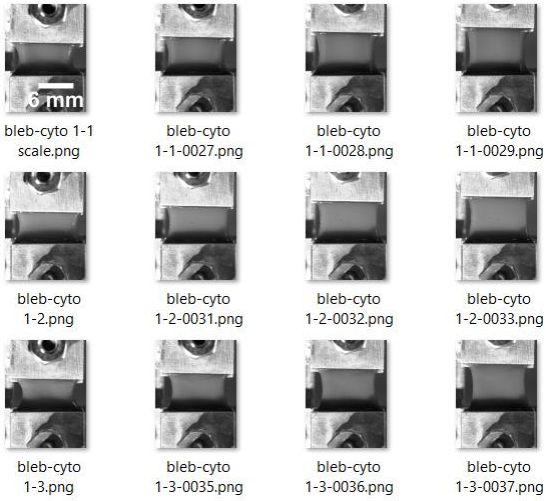

Donor 3 blebbistatin plus cytochalasin mixture top-view images

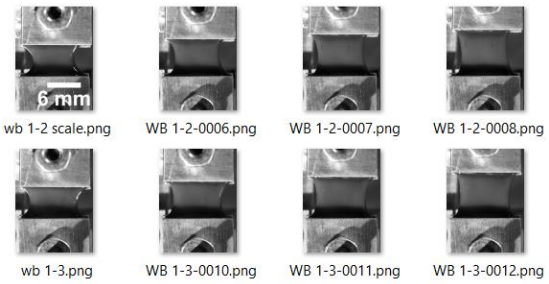

Donor 4 whole blood top-view images

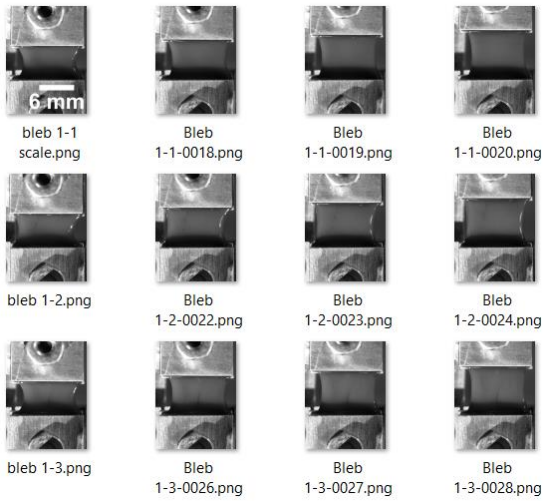

Donor 4 blebbistatin top-view images

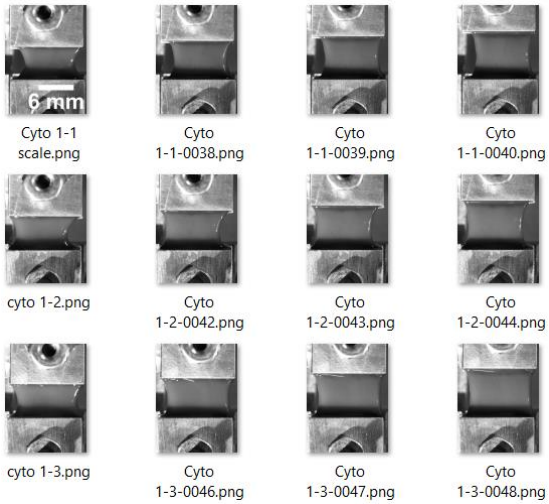

Donor 4 cytochalasin top-view images

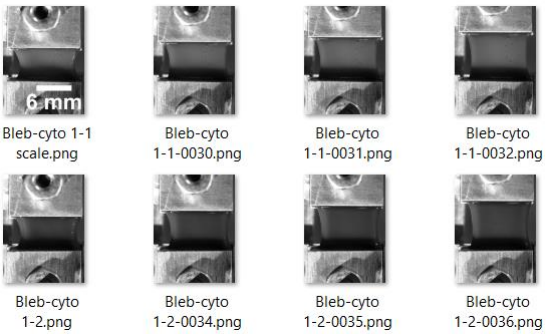

Donor 4 blebbistatin plus cytochalasin mixture top-view images

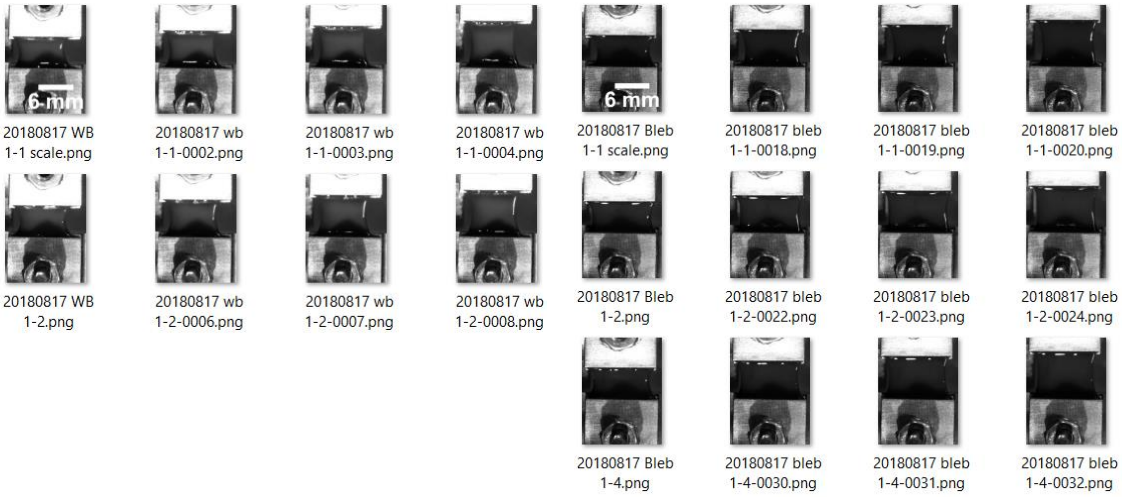

Donor 5 whole blood top-view images

Donor 5 blebbistatin top-view images

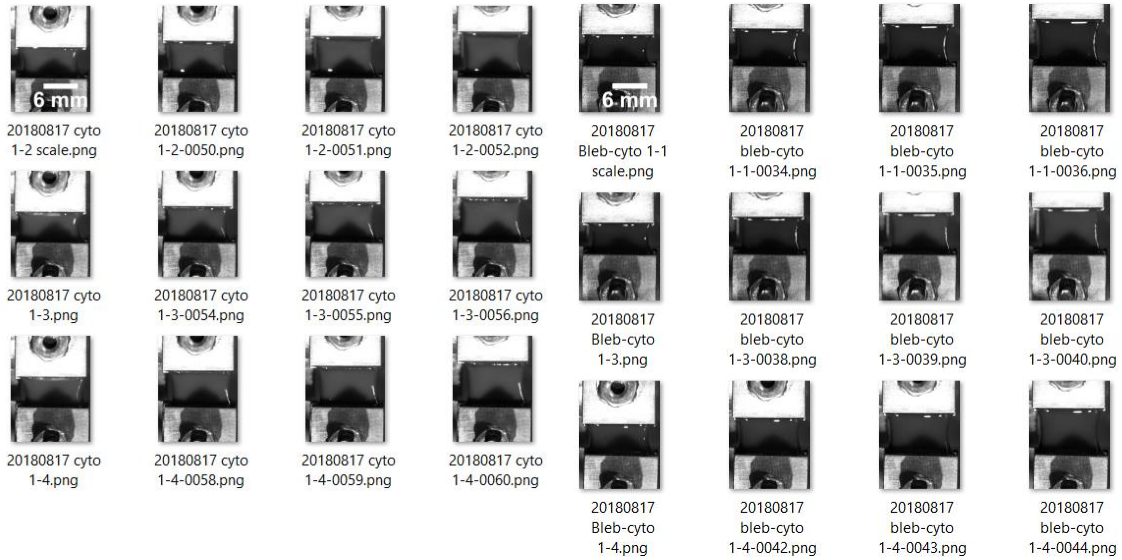

Donor 5 cytochalasin top-view images

Donor 5 blebbistatin plus cytochalasin mixture top-view images

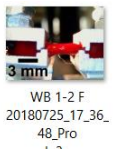

WB 1-2 F 20180725_17_36_48_Pro

WB 1-2 L 20180725_17_38_00_Pro.jpg

WB 1-4 F 20180725_17_51_55_Pro.jpg

WB 1-4 L 20180725_17_53_10_Pro.jpg

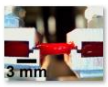

Bleb 1-2 F 20180725_18_14_39_Pro scale.jpg

Bleb 1-2 L 20180725_18_15_18_Pro.jpg

Bleb 1-4 F 20180725_18_30_30_Pro.jpg

Bleb 1-4 L 20180725_18_31_35_Pro.jpg

Donor 1 whole blood side-view images

Donor 1 blebbistatin side-view images

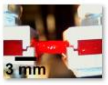

Cyto 1-1 F 20180725_19_32_17_Pro scale.png

Cyto 1-1 L 20180725_19_33_49_Pro.jpg

Cyto 1-2 F 20180725_19_40_29_Pro.jpg

Cyto 1-2 L 20180725_19_42_05_Pro.jpg

Cyto 1-3 F 20180725_19_48_46_Pro.jpg

Cyto 1-3 L 20180725_19_50_00_Pro.jpg

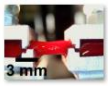

B-C 1-1 F 20180725_18_53_06_Pro scale.jpg

B-C 1-1 L 20180725_18_54_25_Pro.jpg

B-C 1-3 F 20180725_19_08_13_Pro.jpg

B-C 1-3 L 20180725_19_09_27_Pro scale.png

B-C 1-4 F 20180725_19_15_27_Pro.jpg

B-C 1-4 L 20180725_19_17_09_Pro.jpg

Donor 1 cytochalasin side-view images

Donor 1 blebbistatin plus cytochalasin mixture side-view images

WB 1-1 F 20180727_17_19_25_Pro scale.jpg

WB 1-1 L 20180727_17_19_25_Pro.jpg

WB 1-2 F 20180727_17_25_30_Pro.jpg

WB 1-2 L 20180727_17_26_44_Pro.jpg

WB 1-3 F 20180727_17_32_25_Pro.jpg

WB 1-3 L 20180727_17_33_50_Pro.jpg

Bleb 1-1 F 20180727_17_55_35_Pro scale.jpg

Bleb 1-1 L 20180727_17_57_02_Pro.jpg

Bleb 1-3 F 20180727_18_11_15_Pro.jpg

Bleb 1-3 L 20180727_18_12_22_Pro.jpg

Bleb 1-4 F 20180727_18_18_51_Pro.jpg

Bleb 1-4 L 20180727_18_19_39_Pro.jpg

Donor 2 whole blood side-view images

Donor 2 blebbistatin side-view images

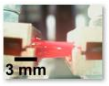

Cyto 1-1 F 20180727_19_15_16_Pro scale.jpg

Cyto 1-1 L 20180727_19_16_17_Pro.jpg

Cyto 1-3 F 20180727_19_28_34_Pro.jpg

Cyto 1-3 L 20180727_19_29_48_Pro.jpg

Cyto 1-4 F 20180727_19_35_13_Pro.jpg

Cyto 1-4 L 20180727_19_36_43_Pro.jpg

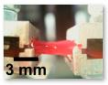

B-C 1-1 F 20180727_18_36_01_Pro scale.jpg

B-C 1-1 L 20180727_18_37_23_Pro.jpg

B-C 1-3 F 20180727_18_43_38_Pro.jpg

B-C 1-3 L 20180727_18_44_54_Pro.jpg

B-C 1-4 F 20180727_18_52_00_Pro.jpg

B-C 1-4 L 20180727_18_53_11_Pro.jpg

Donor 2 cytochalasin side-view images

Donor 2 blebbistatin plus cytochalasin mixture side-view images

WB 1-1 F 20180731_17_21_49_Pro scale.jpg


WB 1-1 L 20180731_17_23_29_Pro.jpg


WB 1-2 F 20180731_17_29_03_Pro.jpg


WB 1-2 L 20180731_17_30_20_Pro.jpg


WB 1-3 F 20180731_17_36_29_Pro.jpg


WB 1-3 L 20180731_17_37_08_Pro.jpg

Donor 3 whole blood side-view images

Bleb 1-1 F 20180731_18_00_56_Pro scale.jpg


Bleb 1-1 F 20180731_18_01_10_Pro.jpg


Bleb 1-1 L 20180731_18_02_52_Pro.jpg


Bleb 1-3 F 20180731_18_18_14_Pro.jpg


Bleb 1-3 F 20180731_18_19_44_Pro.jpg


Bleb 1-3 L 20180731_18_20_17_Pro.jpg

Donor 3 blebbistatin side-view images

Cyto 1-1 F 20180731_19_27_59_Pro scale.jpg


Cyto 1-1 L 20180731_19_29_36_Pro.jpg


Cyto 1-2 F 20180731_19_35_40_Pro.jpg


Cyto 1-2 L 20180731_19_36_28_Pro.jpg


Cyto 1-3 F 20180731_19_41_46_Pro.jpg


Cyto 1-3 L 20180731_19_43_03_Pro.jpg

Donor 3 cytochalasin side-view images

B-C 1-1 F 20180731_18_42_52_Pro scale.jpg


B-C 1-1 L 20180731_18_44_26_Pro.jpg


B-C 1-2 F 20180731_18_49_56_Pro.jpg


B-C 1-2 L 20180731_18_51_52_Pro.jpg


B-C 1-3 F 20180731_18_58_30_Pro.jpg


B-C 1-3 L 20180731_19_00_05_Pro.jpg

Donor 3 blebbistatin plus cytochalasin mixture side-view images

WB 1-2 F 20180801_17_25_58_Pro scale.jpg


WB 1-2 L 20180801_17_27_15_Pro.jpg


WB 1-3 F 20180801_17_33_39_Pro.jpg


WB 1-3 L 20180801_17_35_04_Pro.jpg

Bleb 1-1 F 20180801_17_54_30_Pro scale.jpg


Bleb 1-1 L 20180801_17_56_19_Pro.jpg


Bleb 1-2 F 20180801_18_01_44_Pro.jpg


Bleb 1-2 L 20180801_18_03_34_Pro.jpg


Bleb 1-3 F 20180801_18_10_44_Pro.jpg


Bleb 1-3 L 20180801_18_11_52_Pro.jpg

Donor 4 whole blood side-view images

Donor 4 blebbistatin side-view images

Cyto 1-1 F 20180801_19_17_53_Pro scale.jpg


Cyto 1-1 L 20180801_19_19_59_Pro.jpg


Cyto 1-2 F 20180801_19_25_34_Pro.jpg


Cyto 1-2 L 20180801_19_26_50_Pro.jpg


Cyto 1-3 F 20180801_19_32_26_Pro.jpg


Cyto 1-3 L 20180801_19_33_45_Pro.jpg

Donor 4 cytochalasin side-view images

B-C 1-1 F 20180801_18_36_15_Pro scale.jpg

B-C 1-1 L 20180801_18_37_48_Pro.jpg

B-C 1-2 F 20180801_18_45_01_Pro.jpg

B-C 1-2 L 20180801_18_46_10_Pro.jpg

Donor 4 blebbistatin plus cytochalasin mixture side-view images

Donor 5 whole blood side-view images

Donor 5 blebbistatin side-view images

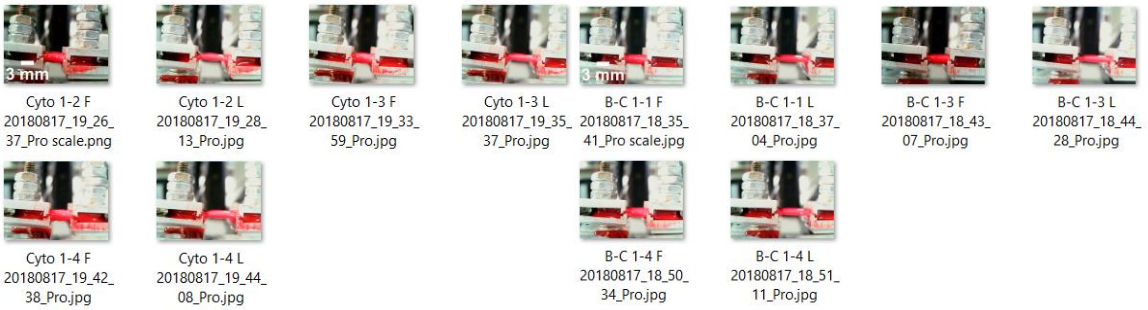

Donor 5 cytochalasin side-view images

Donor 5 blebbistatin plus cytochalasin mixture side-view images